Available online at www.sciencedirect.com
SCIENCE DIRECT®
Comput. Methods Appl. Mech. Engrg. 192 (2003) 1337–1375
Computer methods in applied mechanics and engineering
www.elsevier.com/locate/cma

Perfectly matched layers for time-harmonic elastodynamics of unbounded domains: theory and finite-element implementation

Ushnish Basu, Anil K. Chopra *

Department of Civil and Environmental Engineering, University of California, 707 Davis Hall, Berkeley, CA 94720-1710, USA

Received 3 June 2002; received in revised form 27 November 2002

Abstract

One approach to the numerical solution of a wave equation on an unbounded domain uses a bounded domain surrounded by an absorbing boundary or layer that absorbs waves propagating outwards from the bounded domain. A perfectly matched layer (PML) is an unphysical absorbing layer model for linear wave equations that absorbs, almost perfectly, outgoing waves of all non-tangential angles-of-incidence and of all non-zero frequencies. This paper develops the PML concept for time-harmonic elastodynamics in Cartesian coordinates, utilising insights obtained with electromagnetics PMLs, and presents a novel displacement-based, symmetric finite-element implementation of the PML for time-harmonic plane-strain or three-dimensional motion. The PML concept is illustrated through the example of a one-dimensional rod on elastic foundation and through the anti-plane motion of a two-dimensional continuum. The concept is explored in detail through analytical and numerical results from a PML model of the semi-infinite rod on elastic foundation, and through numerical results for the anti-plane motion of a semi-infinite layer on a rigid base. Numerical results are presented for the classical soil–structure interaction problems of a rigid strip-footing on a (i) half-plane, (ii) layer on a half-plane, and (iii) layer on a rigid base. The analytical and numerical results obtained for these canonical problems demonstrate the high accuracy achievable by PML models even with small bounded domains.

Keywords: Perfectly matched layers; Absorbing boundary; Helmholtz equation; Elastic waves; Frequency domain; Finite elements

1. Introduction

Solution of wave equations over unbounded domains is of interest in various fields of both science and engineering [1,2]. In particular, solution of the elastodynamic wave equation on an unbounded domain finds applications in soil–structure interaction analysis [3] and in the simulation of earthquake ground

* Corresponding author. Tel.: +1-510-642-1292; fax: +1-510-643-8928.
E-mail address: chopra@ce.berkeley.edu (A.K. Chopra).

0045-7825/03/$ - see front matter
doi:10.1016/S0045-7825(02)00642-4

Nomenclature

a_0	non-dimensional frequency
A	cross-sectional area of elastic rod
b	half-width of footing
$\mathbf{B}_I$, $\widetilde{\mathbf{B}}_I$	nodal compatibility matrices
c	damping coefficient of $\overline{S}$, $\overline{S}^{\infty}$
c_{l}	wave velocity in elastic rod
c_{p}	P-wave velocity
c_{s}	S- or shear-wave velocity
c_{v}	Love-wave velocity
$\mathbf{C}$, C_{ijkl}	material stiffness tensor
d	depth of layer
$\mathbf{D}$	material moduli matrix
$\{\boldsymbol{e}_i\}$	standard orthonormal basis
E, E^*	Young's modulus
f, $\bar{f}$, f_i, f^{e}, f^{p}	attenuation function(s)
f_{m}	see Eq. (59)
F, $\overline{F}$, F_i, $\overline{F}^{\mathrm{e}}$, $\overline{F}^{\mathrm{p}}$	integrals of f, $\bar{f}$, f_i, f^{e}, f^{p}
F_{ij}	flexibility coefficient of rigid strip-footing, with $i,j \in \{V,H,R\}$
$\mathbf{F}^{\infty}$	dynamic flexibility matrix of rigid strip-footing
H	(in subscript) horizontal DOF of rigid strip-footing
$\mathrm{i} = \sqrt{-1}$	unit imaginary number
Im	imaginary part of a complex number
$\mathbf{I}$	identity matrix
k	stiffness coefficient of $\overline{S}$, $\overline{S}^{\infty}$
k_g, k_g^*	static stiffness per unit length of (visco)elastic foundation of rod
k_{p}, k_{s}, k_{v}	wave numbers for P, S, and Love waves
$\mathbf{k}^{\mathrm{e}}_{IJ}$	nodal submatrix of element stiffness matrix
L	length of bounded medium
L_P	depth of PML
$\mathbf{m}^{\mathrm{e}}_{IJ}$	nodal submatrix of element mass matrix
$\boldsymbol{n}$	unit normal to a surface
$\boldsymbol{N}$, N_I	nodal shape functions
$\boldsymbol{p}$, p_i	direction of wave propagation
$\boldsymbol{q}$	direction of particle motion
$\mathbf{Q}$, Q_{ij}	rotation-of-basis matrix
r_0	characteristic length quantity for the rod on elastic foundation
R	(in subscript) rocking DOF of rigid strip-footing
$\lvert R\rvert$, $\lvert R_{\mathrm{pp}}\rvert$, $\lvert R_{\mathrm{sp}}\rvert$	amplitude(s) of wave(s) reflected from the PML
Re	real part of a complex number
$\overline{S}$	non-dimensional dynamic stiffness of bounded rod
$\overline{S}^{\infty}$	non-dimensional dynamic stiffness of unbounded rod
S_{ij}	component of dynamic stiffness matrix of layer on rigid base
$\mathbf{S}^{\infty}$	dynamic stiffness matrix of layer on rigid base
u, u_i, $\boldsymbol{u}$	displacement(s)

V (in subscript) vertical DOF of rigid strip-footing
w, w_i, $\boldsymbol{w}$ arbitrary weighting function in weak form
x, x_i, $\boldsymbol{x}$ real coordinate(s)
$\tilde{x}$, $\tilde{x}_i$, $\tilde{\boldsymbol{x}}$ complex stretched coordinate(s)

Greek symbols

δ_{ij} Kronecker delta
ε, ε_i, ε_{ij}, $\boldsymbol{\varepsilon}$ infinitesimal strain tensor (scalar for one-dimensional and vector for anti-plane)
ζ hysteretic damping ratio for viscoelastic medium
θ angle of incidence of outgoing wave on perfectly matched layer (PML)
κ, κ^* bulk modulus
λ, λ_i complex coordinate stretching function(s)
$\widetilde{\boldsymbol{\Lambda}}$, $\widetilde{\Lambda}_{ij}$ left stretch tensor
$\boldsymbol{\Lambda}$, Λ_{ij} right stretch tensor
μ, μ^* shear modulus
v Poisson's ratio
ρ mass density
σ, σ_i, σ_{ij}, $\boldsymbol{\sigma}$ stress tensor (scalar for 1D and vector for anti-plane)
ω excitation frequency
Ω entire bounded domain used for computation
Ω^{e} element domain
Ω_{BD} elastic domain
Ω_{PM} perfectly matched layer
$\Omega^{\infty}_{\mathrm{PM}}$ unbounded perfectly matched medium (PMM)

motion [4], since the ground beneath a structure or a geographical area of interest can be rationally modelled as an unbounded elastic domain.

Solution of a wave equation in an unbounded domain requires the imposition of a radiation condition in any unbounded direction: waves should radiate outwards from a source—a vibrating structure, for example—toward an unbounded direction, without any spurious wave motion in the reverse direction. Irregularities in the geometry of the domain or in the physical material often compel a numerical solution of the problem, thus requiring the use of a bounded domain, along with an artificial boundary that absorbs outgoing waves, for the modelling of the unbounded domain. Typical absorbing boundaries belong to one of two broad categories: (1) rigorous, non-local boundaries [5–8], or (2) approximate, local boundaries [9–11]. The various absorbing boundaries, local or not, are not without drawbacks. The rigorous boundaries are highly accurate and thus may be used with a small bounded domain. However, the low computational cost due to the small size of the domain may be negated by the expense due to not only the non-local nature of such boundaries but also the computation of the boundary terms. Moreover, rigorous boundaries may not be available for all problems of interest. The approximate boundaries, although local and cheaply computed, may require large bounded domains for satisfactory accuracy, since typically they absorb incident waves well only over a small range of angles-of-incidence. Moreover, high-order approximate boundaries require the use of special finite elements [12,13] for proper implementation. Various absorbing layer models [14–16] surrounding a bounded elastic domain have also been proposed as alternatives to absorbing boundaries; however, obtaining satisfactory performance from such

models may require careful formulation and implementation, since the change in material properties from the elastic medium to the absorbing layer causes reflection of incident waves [17]. Also notable are special absorbing boundaries such as the superposition boundary [18] and infinite elements [19,20]; although based on interesting ideas, use of these boundaries may prove to be cumbersome and may be computationally expensive.

A perfectly matched layer (PML) is an absorbing layer model for linear wave equations that absorbs, almost perfectly, propagating waves of all non-tangential angles-of-incidence and of all non-zero frequencies. The concept of a PML was first introduced by Bérenger [21] in the context of electromagnetic waves. More significantly, Chew and Weedon [22] showed – almost immediately – that the Bérenger PML equations arise from a complex-valued coordinate stretching in the electromagnetic wave equations. Since the introduction of these seminal ideas, extensive research has been conducted on various aspects of PMLs for electromagnetic waves; this is mentioned without references: a review of electromagnetics PMLs is beyond the scope of this paper. PMLs have been formulated for other linear wave equations too: the scalar wave equation or the Helmholtz equation [23–25], the linearised Euler equations [26], the wave equation for poroelastic media [27], and, as discussed below, to the elastodynamic wave equation.

To the authors' best knowledge, the idea that PMLs could be formulated for the elastodynamic wave equation was first introduced by Chew and Liu [28]: they used complex-valued coordinate stretching to obtain the equations governing the PML and presented a proof of the absorptive property of the PML. Furthermore, they presented a finite-difference-time-domain (FDTD) formulation obtained through field splitting or an unphysical additive decomposition of the velocity and stress fields. Contemporaneously, Hastings et al. [29] applied Bérenger's original split-field formulation of the electromagnetics PML directly to the P- and S-wave potentials and obtained a two-dimensional FDTD scheme for implementing the resultant formulation. Liu [30] later applied the coordinate stretching idea to the velocity–stress formulation of the elastodynamic equation to obtain split-field PMLs for time-dependent elastic waves in cylindrical and spherical coordinates. Zhang and Ballmann [31] and Collino and Tsogka [32] have also obtained split-field, time-domain PMLs for the velocity–stress formulation and presented FDTD implementations. The latter have also implemented the PML using a two-dimensional mixed finite-element (FE) scheme [33] in which the degrees-of-freedom of each element are the velocity, the shear stress, and split-field components of the axial stresses.

The objective of this paper is twofold: (a) develop the concept of a PML in the context of time-harmonic elastodynamics in Cartesian coordinates, utilising some of the insights obtained in the context of electromagnetics [34–36], and (b) present a novel displacement-based, symmetric FE implementation of the PML for time-harmonic plane-strain or three-dimensional motion. The PML concept is illustrated through the one-dimensional example of a rod on elastic foundation and through the two-dimensional example of the anti-plane motion of a continuum, governed by the Helmholtz equation. The PMLs for these two systems are studied through analytical and numerical (FE) results for the dynamic stiffness of a semi-infinite rod on elastic foundation, and through numerical results for the anti-plane dynamic stiffness of a semi-infinite layer on rigid base. The PML for plane-strain and three-dimensional motion is presented next, together with its FE implementation. Numerical results are presented for the classical soil–structure interaction problems of a rigid strip-footing on a (i) half-plane, (ii) layer on a half-plane, and (iii) layer on a rigid base.

Tensorial and indicial notation will be used interchangeably in this paper; the summation convention will be assumed unless an explicit summation is used or it is mentioned otherwise. An italic boldface symbol will represent a vector, e.g., $\boldsymbol{x}$, an upright boldface symbol will represent a tensor or its matrix in a particular orthonormal basis, e.g., $\mathbf{D}$, and a sans-serif boldface symbol will represent a fourth-order tensor, e.g., C; the corresponding lightface symbols with Roman subscripts will denote components of the tensor, matrix or vector.

2. A one-dimensional system

2.1. Semi-infinite rod on elastic foundation

Consider a semi-infinite rod on elastic foundation (Fig. 1), not subjected to any body forces, but subjected to an imposed displacement $u_0 \exp(\mathrm{i}\omega t)$ at the left end ($x = 0$), and a radiation condition for $x \to \infty$, with ω the frequency of excitation. This excitation causes time-harmonic displacements $u(x)\exp(\mathrm{i}\omega t)$, which are governed by the following equations:

$$\frac{\mathrm{d}\sigma}{\mathrm{d}x} - \frac{k_g}{A}u = -\omega^2 \rho u, \tag{1a}$$

$$\sigma = E\varepsilon, \tag{1b}$$

$$\varepsilon = \frac{\mathrm{d}u}{\mathrm{d}x}, \tag{1c}$$

where σ and ε are the axial stress and infinitesimal strain in the rod, E is the Young's modulus of the rod, A its cross-sectional area, ρ its mass density, and k_g the static stiffness per unit length of the foundation.

The frequency-response of this system can be expressed in terms of a dimensionless frequency $a_0 = \omega r_0/c_1$, where $r_0 = \sqrt{EA/k_g}$ is a characteristic length quantity and $c_1 = \sqrt{E/\rho}$ is the wave velocity in the rod. For $a_0 < 1$, Eq. (1) admits rightward- and leftward-evanescent-wave solutions of the form

$$u(x) = \exp\left[-\sqrt{1-a_0^2}\,\frac{x}{r_0}\right] \quad \text{and} \quad u(x) = \exp\left[+\sqrt{1-a_0^2}\,\frac{x}{r_0}\right], \tag{2}$$

and admits rightward- and leftward-propagating-wave solutions of the form

$$u(x) = \exp\left[-\mathrm{i}\sqrt{a_0^2-1}\,\frac{x}{r_0}\right] \quad \text{and} \quad u(x) = \exp\left[+\mathrm{i}\sqrt{a_0^2-1}\,\frac{x}{r_0}\right] \tag{3}$$

for $a_0 > 1$, with $a_0 = 1$ the cut-off frequency of the system; the radiation condition allows only the rightward modes in the system. The dynamic stiffness at $x = 0$, which is the axial force $-\sigma A$ required in the positive x-direction at $x = 0$ to maintain $u_0 = 1$, can be obtained using Eqs. (1b), (1c), (2a), (3a) as

$$S^{\infty}(a_0) = K^{\infty}\sqrt{1-a_0^2}, \tag{4}$$

where $K^{\infty} = \sqrt{EAk_g}$ is the static stiffness coefficient of the system. The dimensionless dynamic stiffness, corresponding to $K^{\infty} = 1$, is defined as

$$\overline{S}^{\infty}(a_0) := \sqrt{1-a_0^2}. \tag{5}$$

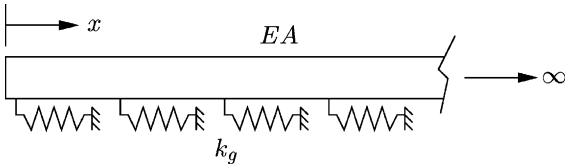

Fig. 1. Homogeneous (visco)elastic semi-infinite rod on elastic foundation.

The motion of a viscoelastic system, where material damping is introduced through the correspondence principle [37], is also described by the above equations, but with complex-valued material moduli $E^* = E(1 + 2i\zeta)$ and $k_g^* = k_g(1 + 2i\zeta)$ in place of the real moduli E and k_g, ζ being the hysteretic damping ratio. The introduction of complex moduli results in a complex-valued wave speed $c_1^* = c_1\sqrt{1 + 2i\zeta}$ and complex-valued dimensionless frequency $a_0^* = a_0/\sqrt{1 + 2i\zeta}$.

The solutions for the displacement and dynamic stiffness of the semi-infinite rod are obtained by analytically solving Eq. (1) on the unbounded domain $[0, \infty)$ using appropriate boundary conditions. Numerical solution of this unbounded domain problem requires the solution of Eq. (1) on a bounded domain augmented by an artificial absorbing boundary or layer; a PML is an absorbing layer model that can be used towards this purpose.

2.2. Perfectly matched medium

Consider a system of equations of the same form as Eq. (1), but with x replaced by a stretched coordinate $\tilde{x}$, defined as [34]

$$\tilde{x} := \int_0^x \lambda(s)\,\mathrm{d}s, \tag{6}$$

where λ is a nowhere-zero, continuous, complex-valued coordinate *stretching function*. By the continuity of λ,

$$\frac{\mathrm{d}\tilde{x}}{\mathrm{d}x} = \lambda(x), \tag{7}$$

which formally implies

$$\frac{\mathrm{d}}{\mathrm{d}\tilde{x}} = \frac{1}{\lambda(x)}\frac{\mathrm{d}}{\mathrm{d}x}. \tag{8}$$

Thus this aforementioned system of equations can be defined as

$$\frac{1}{\lambda(x)}\frac{\mathrm{d}\sigma}{\mathrm{d}x} - \frac{k_g}{A}u = -\omega^2\rho u, \tag{9a}$$

$$\sigma = E\varepsilon, \tag{9b}$$

$$\varepsilon = \frac{1}{\lambda(x)}\frac{\mathrm{d}u}{\mathrm{d}x}, \tag{9c}$$

as a modification of Eq. (1), where the constitutive relation, Eq. (9b), remains the same as for the elastic medium. A perfectly matched medium (PMM) for a rod on elastic foundation is defined to be a medium where the field variable u is governed by Eq. (9). The (visco)elastic medium is a special PMM, where $\lambda(x) \equiv 1$.

Eq. (9) is only motivated by, but defined independently of Eq. (8); using the latter to derive the PMM equations from Eq. (1) would involve issues of complex differentiability, all of which are neatly avoided by the independent definition of the PMM. The assumption of continuity on λ could presumably be dropped, by considering one-sided derivatives, or possibly even weak derivatives, in Eq. (7); such technical issues are avoided by this convenient assumption. Note that the assumption of a continuous λ is not restrictive in the least: the stretching function is specified a priori, and is not a physical quantity that is intrinsically discontinuous.

As is to be expected from the coordinate-stretching motivation, Eq. (9) admits solutions similar in form to those in Eqs. (2) and (3) admitted by the elastic medium, but with x replaced by $\tilde{x}$. Evanescent-wave-type solutions are of the form

$$u(x) = \exp\left[-\sqrt{1-a_0^2}\,\frac{\tilde{x}}{r_0}\right] \quad \text{and} \quad u(x) = \exp\left[+\sqrt{1-a_0^2}\,\frac{\tilde{x}}{r_0}\right] \tag{10}$$

for $a_0 < 1$, and propagating-wave-type solutions are of the form

$$u(x) = \exp\left[-\mathrm{i}\sqrt{a_0^2-1}\,\frac{\tilde{x}}{r_0}\right] \quad \text{and} \quad u(x) = \exp\left[+\mathrm{i}\sqrt{a_0^2-1}\,\frac{\tilde{x}}{r_0}\right] \tag{11}$$

for $a_0 > 1$; that these are solutions of Eq. (9) can be shown by utilising the continuity of λ through Eq. (7).

A special property of these PMMs is that if two PMMs with different λ are placed adjacent to each other, with the functions λ such that they match at the interface of the two media, then a wave-type motion will pass through the interface without generating any reflected wave; this is the *perfect matching* property of the PMM. Without loss of generality, consider two PMMs: one is defined on $(-\infty, 0)$ with $\lambda(x) := \lambda^{\mathrm{lt}}(x)$, and the other on $[0, \infty)$ with $\lambda(x) := \lambda^{\mathrm{rt}}(x)$, with the stretching functions such that $\lambda^{\mathrm{lt}}(0) = \lambda^{\mathrm{rt}}(0)$. These two PMMs can be considered as only one PMM but with a continuous λ defined piecewise on $(-\infty, 0)$ and $[0, \infty)$; thus, there is no interface, precluding the possibility of the generation of any reflected wave. The Perfect matching property holds for both solutions in Eq. (11) as well as for those in Eq. (10), i.e., it is independent of the type of wave, of the direction of propagation, and of the frequency a_0.

Another special property of the PMMs is that for suitable choices of λ, the solutions in the PMM take the form of the corresponding elastic-medium solution but with an imposed spatial attenuation. Consider, for $a_0 > 1$, λ defined in terms of a real-valued, continuous function f as

$$\lambda(x) := 1 - \mathrm{i}\frac{f(x)}{\sqrt{a_0^2-1}}. \tag{12}$$

Then

$$\frac{\tilde{x}}{r_0} = \frac{x}{r_0} - \mathrm{i}\frac{\overline{F}(x/r_0)}{\sqrt{a_0^2-1}}, \tag{13}$$

where

$$\overline{F}(\bar{x}) := \int_0^{\bar{x}} \bar{f}(\bar{\xi})\,\mathrm{d}\bar{\xi}, \tag{14}$$

with $\bar{\xi} = \xi/r_0$ and $\bar{f}(\bar{\xi}) = f(r_0\bar{\xi}) = f(\xi)$. On substituting for $\tilde{x}$ from Eq. (13) into Eq. (11a), the solution is obtained as

$$u(x) = \exp[-\overline{F}(x/r_0)]\exp\left[-\mathrm{i}\sqrt{a_0^2-1}\,\frac{x}{r_0}\right]. \tag{15}$$

Thus, if $\overline{F}(x/r_0) > 0$, then $u(x)$ is a rightward propagating wave that is attenuated in that direction, with the attenuation independent of the frequency due to the choice of $\lambda(x)$; the function f is termed the *attenuation function*. Furthermore, for $a_0 < 1$, consider λ defined as

$$\lambda(x) := 1 + \frac{f(x)}{\sqrt{1-a_0^2}}; \tag{16}$$

then Eq. (10a) is transformed to

$$u(x) = \exp[-\overline{F}(x/r_0)] \exp\left[- \sqrt{1 - a_0^2} \frac{x}{r_0} \right], \tag{17}$$

i.e., an evanescent wave with additional attenuation.

The above choices for the stretching function are merely illustrative choices that exploit prior knowledge of the solution. A more realistic choice for λ would be in terms of two non-negative attenuation functions f^{e} and f^{p}, as

$$\lambda(x) := \left[1 + \frac{f^{\mathrm{e}}(x)}{a_0} \right] - \mathrm{i} \frac{f^{\mathrm{p}}(x)}{a_0}. \tag{18}$$

This function does not assume knowledge of the frequency equation of the system, nor does a priori distinguish between evanescent and propagating waves. This choice for λ imposes a frequency-dependent attenuation and a phase change on the rightward propagating wave: Eq. (11a) is transformed into

$$u(x) = \exp\left[- \overline{F}^{\mathrm{p}}(x/r_0) \sqrt{1 - \frac{1}{a_0^2}} \right] \exp\left[- \mathrm{i} \sqrt{a_0^2 - 1} \left(\frac{x}{r_0} + \frac{\overline{F}^{\mathrm{e}}(x/r_0)}{a_0} \right) \right], \tag{19}$$

where $\overline{F}^{\mathrm{e}}$ and $\overline{F}^{\mathrm{p}}$ are appropriately-defined integrals of f^{e} and f^{p}, respectively. Using Eq. (18) imposes an attenuation and a harmonic mode on evanescent waves: Eq. (10a) transforms to

$$u(x) = \exp\left[- \overline{F}^{\mathrm{e}}(x/r_0) \sqrt{\frac{1}{a_0^2} - 1} \right] \exp\left[\mathrm{i} \overline{F}^{\mathrm{p}}(x/r_0) \sqrt{\frac{1}{a_0^2} - 1} \right] \exp\left[- \sqrt{1 - a_0^2} \frac{x}{r_0} \right]. \tag{20}$$

Thus, f^{e} imposes an attenuation on evanescent waves and f^{p} on propagating waves.

2.3. Perfectly matched layer

These special properties of the PMM can be used to define an absorbing layer adjacent to a bounded domain such that the layer and the domain together model the unbounded domain.

Consider the system shown in Fig. 2(a): Ω_{BD} ($:= [0, L]$) is the bounded domain governed by Eq. (1), and $\Omega_{\mathrm{PM}}^{\infty}$ ($:= (L, \infty)$) is the unbounded PMM, governed by Eq. (9). The stretch λ is taken to be of the form in Eq. (12) for $a_0 > 1$ and Eq. (16) for $a_0 < 1$, with f chosen such that $f(L) = 0$. Alternatively, λ can be chosen as in Eq. (18) for all a_0, with the attenuation functions such that $f^{\mathrm{e}}(L) = f^{\mathrm{p}}(L) = 0$. Since the medium in Ω_{BD} is a special PMM, ($\lambda(x) \equiv 1$) and since the admissible choices of attenuation functions impose that the functions λ for the two domains are matched at the interface, all waves propagating outwards from Ω_{BD} are

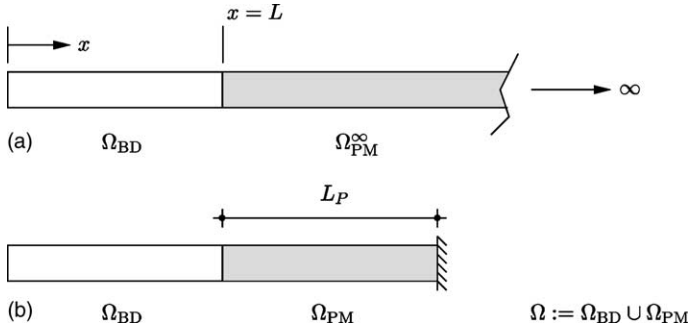

Fig. 2. (a) Perfectly matched medium; (b) Perfectly matched layer, adjacent to the bounded domain for the semi-infinite rod on elastic foundation.

completely absorbed into and then attenuated in $\Omega_{\mathrm{PM}}^{\infty}$. Thus, the displacements of this system in Ω_{BD} are exactly the same as the displacements of the semi-infinite rod in Ω_{BD}.

If the waves are attenuated enough in a finite distance, $\Omega_{\mathrm{PM}}^{\infty}$ can be terminated with a fixed boundary condition at that distance without any significant reflection of the waves. Shown in Fig. 2(b), this bounded PMM Ω_{PM} $(:= (L, L + L_P])$ is termed the PML. If the wave reflection from the fixed boundary is not significant, the displacements of the entire bounded system Ω $(:= \Omega_{\mathrm{BD}} \cup \Omega_{\mathrm{PM}})$ in Ω_{BD} should be almost the same as the displacements of the semi-infinite rod in Ω_{BD}.

2.4. Effect of fixed-end termination of the PML

The effect of domain termination in the PMM is studied analytically, first by calculating the amplitude of waves reflected back from the fixed boundary and then by investigating the effects of L, L_P and f on the (normalised) dynamic stiffness $\overline{S}(a_0)$ of Ω at $x = 0$.

The reflected-wave amplitude is calculated by considering a PMM defined on $[0, L_P]$ with an imposed displacement $u(L_P) = 0$. The stretch is chosen as in Eq. (12) for $a_0 > 1$ and as in Eq. (16) for $a_0 < 1$. A rightward propagating wave ($a_0 > 1$) with an unit amplitude as it enters the PML, alongwith a wave reflected back from the fixed boundary, can be represented as

$$u(x) = \exp\left[-\mathrm{i}\sqrt{a_0^2 - 1}\,\frac{\tilde{x}}{r_0}\right] + R\exp\left[+\mathrm{i}\sqrt{a_0^2 - 1}\,\frac{\tilde{x}}{r_0}\right]. \tag{21}$$

Imposing $u(L_P) = 0$ gives

$$|R| = \exp[-2\overline{F}(L_P/r_0)], \tag{22}$$

which is the amplitude of the reflected wave as it exits the PML. A similar calculation for evanescent waves using Eq. (16) shows that $|R|$ in Eq. (22) is the additional attenuation imposed by the PML on the reflected evanescent wave. This reflection coefficient $|R|$ due to the PML is controlled by the choice of the parameters f and L_P, independently of the size of the bounded domain to which the PML is adjacent. This suggests that if displacement and stress quantities near $x = 0$ for the semi-infinite elastic medium are the quantities of interest in the analysis, the bounded domain may be restricted to the region of interest, thus lowering the computational cost, if the parameters of the PML are chosen appropriately.

A choice of λ as in Eq. (18) leads to

$$|R| = \exp\left[-2\overline{F}^{\mathrm{p}}(L_P/r_0)\sqrt{1 - \frac{1}{a_0^2}}\right] \tag{23}$$

for $a_0 > 1$, and

$$|R| = \exp\left[-2\overline{F}^{\mathrm{e}}(L_P/r_0)\sqrt{\frac{1}{a_0^2} - 1}\right]\exp\left[-2\sqrt{1 - a_0^2}\,\frac{L_P}{r_0}\right] \tag{24}$$

for $a_0 < 1$; an additional attenuation is imposed upon evanescent waves.

The dynamic stiffness of Ω at $x = 0$ is calculated as follows: (1) assume a solution of the form

$$u(x) = B_1\exp\left[-\sqrt{1 - a_0^2}\,\frac{\tilde{x}}{r_0}\right] + B_2\exp\left[+\sqrt{1 - a_0^2}\,\frac{\tilde{x}}{r_0}\right], \tag{25}$$

in terms of constants B_1 and B_2, with imaginary square roots for $a_0 > 1$, and λ in $\tilde{x}$ defined as

$$\lambda(x) \equiv 1 \quad \text{for } x \in [0, L], \tag{26a}$$

and, following Eqs. (16) and (12), in terms of a non-negative attenuation function f as

$$\lambda(x) = \begin{cases} 1 + f(x-L)/\sqrt{1-a_0^2} & \text{if } a_0 < 1 \\ 1 - \mathrm{i} f(x-L)/\sqrt{a_0^2-1} & \text{if } a_0 > 1 \end{cases} \quad \text{for } x \in (L, L+L_P], \tag{26b}$$

(2) impose boundary conditions $u(0) = 1$ and $u(L+L_P) = 0$ to calculate B_1 and B_2, and (3) compute the dynamic stiffness as $-(\sigma A)|_{x=0}$ using Eqs. (9b) and (9c). The dimensionless dynamic stiffness of Ω is thus obtained as

$$\overline{S}(a_0) = \overline{S}^{\infty}(a_0) \frac{1 + |R| \exp\left[-2\sqrt{1-a_0^2}(L+L_P)/r_0\right]}{1 - |R| \exp\left[-2\sqrt{1-a_0^2}(L+L_P)/r_0\right]}, \tag{27}$$

with $\overline{S}^{\infty}(a_0)$ given by Eq. (5), $|R|$ given by Eq. (22). Here $\overline{S}(a_0) \to \overline{S}^{\infty}(a_0)$ as $|R| \to 0$, i.e., the dynamic stiffness of the entire bounded domain is a good approximation to that of the unbounded domain if the reflection coefficient is suitably small.

If λ is chosen as

$$\lambda(x) = \left[1 + \frac{f^{\mathrm{e}}(x-L)}{a_0}\right] - \mathrm{i}\frac{f^{\mathrm{p}}(x-L)}{a_0}, \tag{28}$$

in $(L, L+L_p]$, following Eq. (18), then the dynamic stiffness for all a_0 is still given by Eq. (27), but with $|R|$ replaced by

$$\exp\left[-2\overline{F}^{\mathrm{e}}(L_P/r_0)\sqrt{\frac{1}{a_0^2}-1}\right] \exp\left[2\mathrm{i}\overline{F}^{\mathrm{p}}(L_P/r_0)\sqrt{\frac{1}{a_0^2}-1}\right].$$

Thus, the accuracy of the bounded-domain approximation is controllable through f^{e} for evanescent waves and through f^{p} for propagating waves.

2.5. Effect of PML parameters on accuracy of results

Eq. (27), with $|R|$ given by Eq. (22), is used to investigate the effect of the PML parameters L_P and f on the dynamic stiffness $\overline{S}(a_0)$, represented in terms of frequency-dependent stiffness, $k(a_0)$, and damping, $c(a_0)$, coefficients given by the relation

$$\overline{S}(a_0) = k(a_0) + \mathrm{i}a_0 c(a_0). \tag{29}$$

This approximation to the stiffness of the unbounded medium is compared against the exact stiffness $\overline{S}^{\infty}(a_0)$, also decomposed into stiffness and damping coefficients.

To facilitate a meaningful discussion of the effects of these parameters, the attenuation function is chosen to be of the form

$$f(x) := f_0 \left(\frac{x}{L_P}\right)^m, \tag{30}$$

which gives

$$\overline{F}(L_P/r_0) = \frac{f_0(L_P/r_0)}{m+1}. \tag{31}$$

Thus the reflection coefficient $|R|$ in Eq. (22) depends on the maximum value of the attenuation function, $f_0[= f(L_P)]$, the depth of the PML, L_P/r_0, and the degree of the polynomial attenuation function, m. Eq. (31) suggests that the accuracy will be related directly to f_0 and to L_P/r_0, but inversely to m.

It is demonstrated that it is the depth L_P of the PML that is significant, rather than the size L of the bounded domain. Fig. 3(a) shows that if L_P/r_0 is not large enough, then increasing L/r_0 does not improve

the accuracy of the results. However, as shown in Fig. 3(b), for a sufficiently large PML ($L_P/r_0 = 1$), the size of the bounded domain does not affect the results: in the "eye-norm", there is no difference between either approximate result and the exact one.

Fig. 4 shows the effect of the choice of the attenuation function on the accuracy of results. As was predicted from Eq. (31), increasing f_0 increases the accuracy of results, but increasing m leads to less accurate results. This suggests that the attenuation function should be chosen as a linear polynomial and that the accuracy should be controlled through f_0. An adequate value of f_0 can be established through a rudimentary trial-and-error procedure; it is not appropriate to choose a value of f_0 by choosing an adequate value of $|R|$ in e.g., Eq. (22), because adequacy of the value of $|R|$ is equivalent to adequacy of the value of f_0.

If the dynamic stiffness of the bounded domain is calculated for λ in the PML given by Eq. (28) with $f^{\mathrm{e}} = f^{\mathrm{p}} = f$, then the effects of L, L_P, f_0 and m on the dynamic stiffness is qualitatively similar to their effects for λ in the PML given by Eq. (26b), shown in Figs. 3 and 4; therefore, these results are not presented here. In fact, a highly accurate dynamic stiffness is still obtained by choosing the parameter values $L/r_0 = 1/2$, $L_P/r_0 = 1$, $f_0 = 10$ and $m = 1$.

Although not presented here, accurate results are also obtainable for a viscoelastic rod, for either of the choices of λ given above.

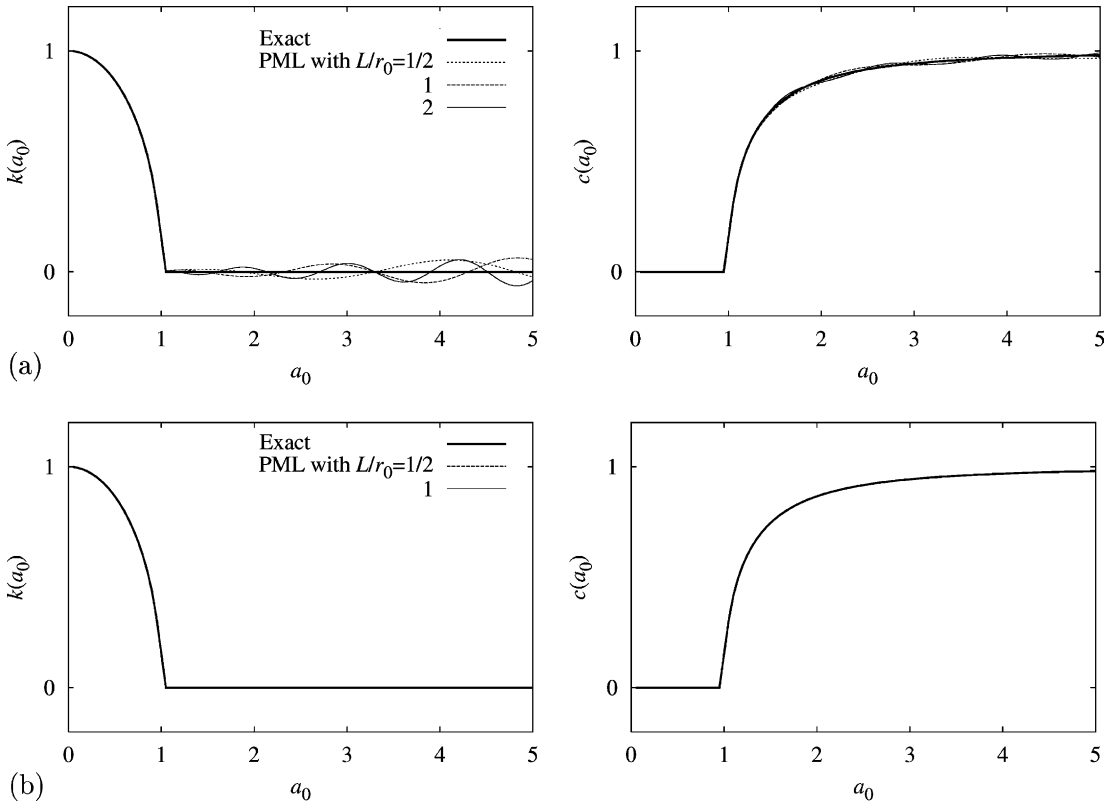

Fig. 3. Effect of size of bounded domain on the accuracy of dynamic stiffness of the elastic rod for two different depths of the PML; $f_0 = 10$, $m = 1$: (a) $L_P/r_0 = 1/2$ and (b) $L_P/r_0 = 1$.

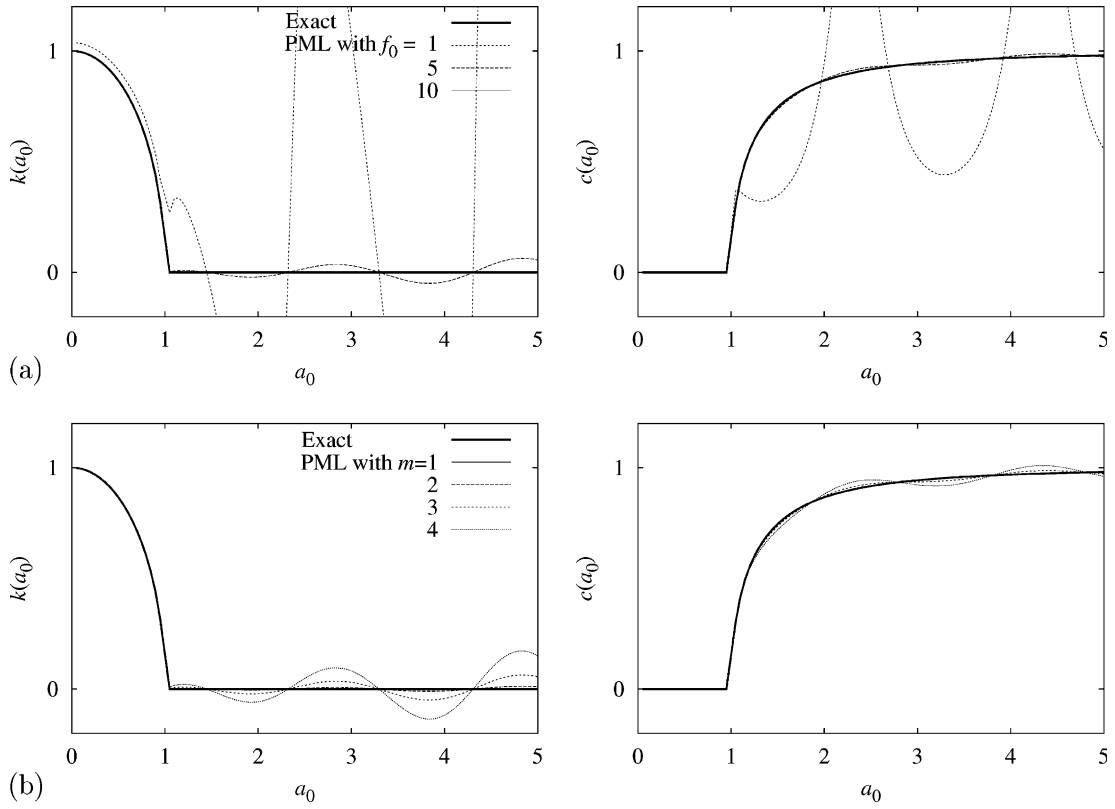

Fig. 4. Effect of attenuation function on the accuracy of dynamic stiffness of the elastic rod; $L/r_0 = 1/2$, $L_P/r_0 = 1$: (a) $m = 1$ and (b) $f_0 = 10$.

2.6. Finite-element implementation

The PMM is equivalently interpreted as an inhomogeneous viscoelastic medium, which is then implemented using standard displacement-based finite elements [38]. Because the displacement formulation is well known, only the salient steps of the implementation are presented.

Eq. (9) is rewritten as follows: Eq. (9a) is multiplied by $\lambda(x)$, and ε in Eq. (9c) is redefined as $\varepsilon \leftarrow \lambda(x)\varepsilon$ to obtain an equivalent system of equations

$$\frac{\mathrm{d}\sigma}{\mathrm{d}x} - \frac{k_g}{A}\lambda(x)u = -\omega^2\rho\lambda(x)u, \tag{32a}$$

$$\sigma = E\frac{1}{\lambda(x)}\varepsilon, \tag{32b}$$

$$\varepsilon = \frac{\mathrm{d}u}{\mathrm{d}x}. \tag{32c}$$

Here, the coordinate stretch has been transformed into a change in the material parameters; this PMM can thus be interpreted to be an inhomogeneous viscoelastic medium.

The weak form of Eq. (32a) is derived as follows: the equation is first multiplied by an arbitrary weighting function, w, residing in an appropriate admissible space, and then integrated over Ω using integration-by-parts to get

$$\int_\Omega \frac{\mathrm{d}w}{\mathrm{d}x}\sigma\,\mathrm{d}\Omega + \int_\Omega \frac{k_g}{A}\lambda(x)wu\,\mathrm{d}\Omega - \omega^2\int_\Omega \rho\lambda(x)wu\,\mathrm{d}\Omega = (w\sigma)|_{\partial\Omega}. \tag{33}$$

The functions u and w are interpolated elementwise in terms of nodal quantities using $\boldsymbol{N}$, a vector of nodal shape functions, and Eqs. (32b) and (32c) are substituted into the integrals on the left hand side of Eq. (33). Restricting the integrals to Ω^{e}, the element domain, gives the stiffness and mass matrices for a PML element:

$$\mathbf{k}^{\mathrm{e}}_{IJ} = \int_{\Omega^{\mathrm{e}}} \frac{\mathrm{d}N_I}{\mathrm{d}x} E \frac{1}{\lambda(x)} \frac{\mathrm{d}N_J}{\mathrm{d}x}\,\mathrm{d}\Omega + \int_{\Omega^{\mathrm{e}}} \frac{k_g}{A}\lambda(x)N_I N_J\,\mathrm{d}\Omega, \tag{34a}$$

$$\mathbf{m}^{\mathrm{e}}_{IJ} = \int_{\Omega^{\mathrm{e}}} \rho\lambda(x)N_I N_J\,\mathrm{d}\Omega; \tag{34b}$$

$\mathbf{k}^{\mathrm{e}}_{IJ}$ and $\mathbf{m}^{\mathrm{e}}_{IJ}$ are the nodal submatrices of the entire element matrices $\mathbf{k}^{\mathrm{e}}$ and $\mathbf{m}^{\mathrm{e}}$, with I and J the node numbers and N_I the shape function corresponding to node I. In Eq. (34), λ is defined globally on the computational domain, not elementwise.

The element stiffness and mass matrices obtained above are symmetric, but are intrinsically complex-valued and frequency-dependent because of the choice for λ (Eq. (12) or Eq. (18)). Hence, the system matrices for Ω will be complex, symmetric, and banded, the PML contributions to which will have to computed anew for each frequency.

2.7. Numerical results

The dynamic stiffness, $\overline{S}(a_0)$, of Ω at $x = 0$, with λ as defined in Eq. (26), is computed using a FE model consisting of two-noded linear isoparametric elements. The mesh is chosen to have n_b elements in a length of r_0 in the bounded domain and n_p elements per r_0 length in the PML; n_b and n_p are parameters in the analysis.

For a sufficiently dense mesh ($n_b = n_p = 30$), the results from the FE model for either choice of λ in the PML (Eq. (26b) or Eq. (28)) match the corresponding analytical results for the dynamic stiffness of the bounded domain, e.g., the results presented in Figs. 3 and 4; therefore, the numerical results are not presented separately.

The effect of mesh density on the accuracy of the computed dynamic stiffness is investigated. Because the mesh should adequately capture significant spatial variations in the displacements, the mesh density in the PML should be governed by both the wavelength and the sharpness of the spatial attenuation. If the spatial attenuation is independent of the frequency, in the case of low frequencies the density should be governed by the sharpness of the attenuation and by the wavelength for high frequencies. The qualifiers "high" and "low" are characterised by the relation of the wavelength to the sharpness of the attenuation. Thus, it should suffice to choose the mesh density in the entire bounded domain to be adequate for a high enough frequency, with the density in the PML similar to that in the bounded domain.

Fig. 5 shows the effect of mesh density in the PML on the accuracy of the dynamic stiffness for two values of n_b. The stiffness coefficient computed with $n_p = n_b = 10$ shows a slight oscillation about the exact solution, with its amplitude increasing with frequency. Increasing n_p gives accurate results for $a_0 \lessapprox 4$; the error found in the higher frequencies is because $n_b = 10$ is not adequate in that range. The slight deterioration in accuracy of results for $n_p = 4n_b$ over those for $n_p = 2n_b$ may be due to the contrast between the densities in Ω_{BD} and Ω_{PM}. For a larger n_b ($= 20$), both $n_p = n_b$ and $n_p = 2n_b$ give highly accurate results. This demonstrates that if the mesh density in the entire bounded domain is adequate for the range of frequencies considered, the accuracy may not be significantly sensitive to the choice of n_p, provided $n_p \geqslant n_b$.

It is computationally advantageous to choose λ in the PML so that the attenuation does not increase too strongly with frequency, especially for higher frequencies, as is indeed the case for functions λ in both Eq. (26b) and Eq. (28). An alternate choice of

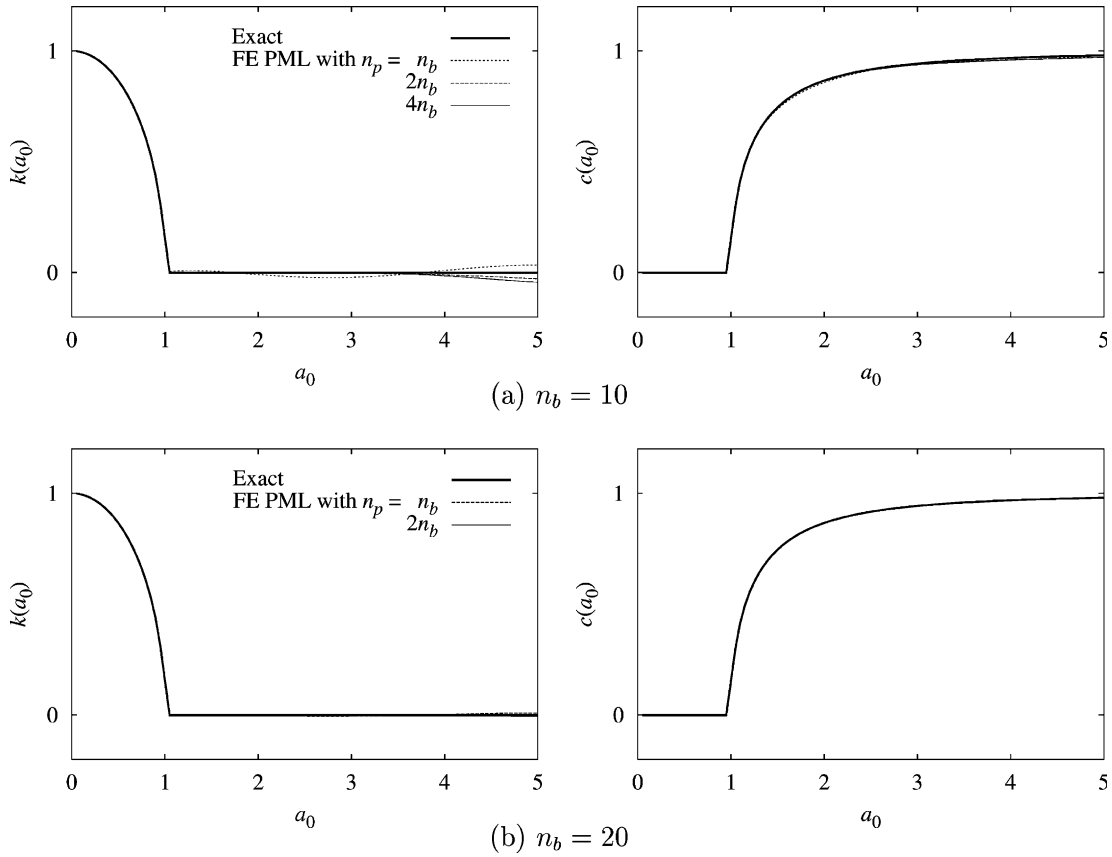

Fig. 5. Effect of mesh density in the PML on accuracy of dynamic stiffness of elastic rod for two different mesh densities in the elastic domain; $L/r_0 = 1/2$, $L_P/r_0 = 1$, $f_0 = 10$, $m = 1$: (a) $n_b = 10$ and (b) $n_b = 20$.

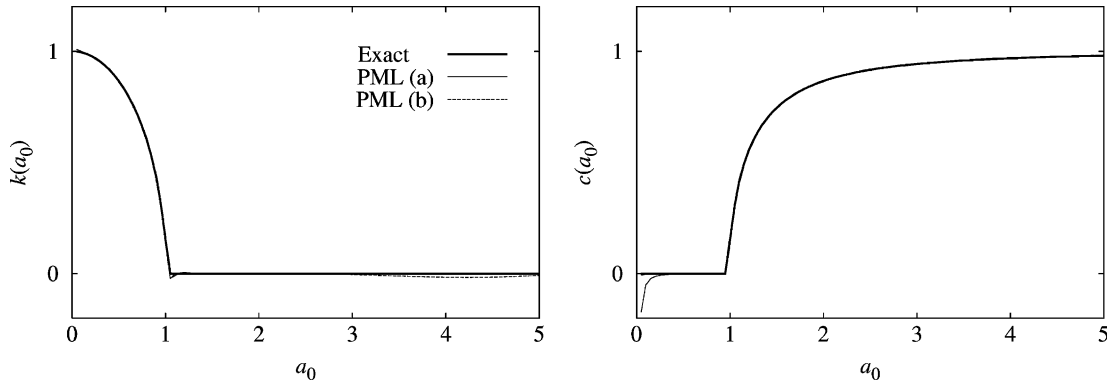

Fig. 6. Effect of frequency dependence of stretching function on the accuracy of the FE solution, with λ in the PML as defined in (a) Eq. (28), and (b) Eq. (35); $n_b = n_p = 30$; $L/r_0 = 1/2$, $L_P/r_0 = 1$, $f_0 = 10$, $m = 1$.

$$\lambda(x) = 1 + f^{\mathrm{e}}(x - L) - \mathrm{i}f^{\mathrm{p}}(x - L) \tag{35}$$

in the PML results in sharper attenuation for higher frequencies, thus requiring higher densities over-and-above the usual high density requirements for high frequencies. As shown in Fig. 6, the FE solution obtained using Eq. (28) is close to the exact result. The error in $c(a_0)$ for very low frequencies is due to the division of $\mathrm{Im}\,\overline{S}(a_0)$ by small values of a_0. In contrast, the FE solution for Eq. (35) does show a slight error in $k(a_0)$ for $a_0 > 3$ which is due to inadequate mesh density in the PML. Although not presented here, this error is not found in either the corresponding analytical solution or the FE solution for a denser PML mesh ($n_b = 30$, $n_p = 60$).

3. Anti-plane motion

3.1. Elastic medium

Consider a two-dimensional homogeneous isotropic elastic continuum undergoing only time-harmonic anti-plane displacements in the absence of body forces. For such motion, if the x_3-direction is taken to point out of the plane, only the 31- and 32-components of the three-dimensional stress and strain tensors are non-zero. The displacements (in the form $u(\boldsymbol{x})\exp(\mathrm{i}\omega t)$, with ω the excitation frequency) are governed by following equations ($i \in \{1, 2\}$):

$$\sum_i \frac{\partial \sigma_i}{\partial x_i} = -\omega^2 \rho u, \tag{36a}$$

$$\sigma_i = \mu \varepsilon_i, \tag{36b}$$

$$\varepsilon_i = \frac{\partial u}{\partial x_i}, \tag{36c}$$

where μ is the shear modulus of the medium and ρ its mass density; σ_i and ε_i represent the $3i$-components of the stress and strain tensors.

On an unbounded domain, Eq. (36) admits plane shear wave solutions [39] of the form

$$u(\boldsymbol{x}) = \exp[-\mathrm{i}k_{\mathrm{s}}\boldsymbol{x}\cdot\boldsymbol{p}], \tag{37}$$

where $k_{\mathrm{s}} = \omega/c_{\mathrm{s}}$ is the wave number, with wave speed $c_{\mathrm{s}} = \sqrt{\mu/\rho}$, and $\boldsymbol{p}$ is a unit vector denoting the propagation direction. Furthermore, consider the domain shown in Fig. 7, which consists of a layer of thickness d with material constants μ_l and ρ_l, with a traction-free surface at $x_1 = -d$, and supported by a half-plane with material constants μ_h and ρ_h. On such a domain, Eq. (36) admits Love-wave solutions of the form

$$u(\boldsymbol{x}) = (B_1\,\mathrm{e}^{-\mathrm{i}\beta_l x_1} + B_2\,\mathrm{e}^{+\mathrm{i}\beta_l x_1})\,\mathrm{e}^{-\mathrm{i}k_{\mathrm{v}}x_2} \quad \text{in the layer,} \tag{38a}$$

$$u(\boldsymbol{x}) = B_3\,\mathrm{e}^{-\beta_h x_1}\mathrm{e}^{-\mathrm{i}k_{\mathrm{v}}x_2} \quad \text{in the half-plane,} \tag{38b}$$

if $c_{\mathrm{s}}^l < c_{\mathrm{s}}^h$, where c_{s}^l and c_{s}^h are the shear wave velocities in the layer and the half-plane respectively. In Eq. (38) B_1, B_2 and B_3 are constants, $\beta_l^2 = (k_{\mathrm{s}}^l)^2 - k_{\mathrm{v}}^2$ and $\beta_h^2 = k_{\mathrm{v}}^2 - (k_{\mathrm{s}}^h)^2$, with $k_{\mathrm{s}}^l = \omega/c_{\mathrm{s}}^l$, $k_{\mathrm{s}}^h = \omega/c_{\mathrm{s}}^h$, and $k_{\mathrm{v}} = \omega/c_{\mathrm{v}}$; c_{v} is the wave speed in the x_2-direction, satisfying $c_{\mathrm{s}}^l < c_{\mathrm{v}} < c_{\mathrm{s}}^h$, and governed by the equation

$$\mu_h\beta_h - \mu_l\beta_l\tan(\beta_l d) = 0. \tag{39}$$

A viscoelastic medium, with damping introduced through the correspondence principle, can also be described using the above equations, but with a complex-valued shear modulus $\mu^* = \mu(1 + 2\mathrm{i}\zeta)$, ζ being the hysteretic damping ratio, leading to a complex-valued wave speed $c_{\mathrm{s}}^* = c_{\mathrm{s}}\sqrt{1 + 2\mathrm{i}\zeta}$ and wave number $k_{\mathrm{s}}^* = k_{\mathrm{s}}/\sqrt{1 + 2\mathrm{i}\zeta}$.

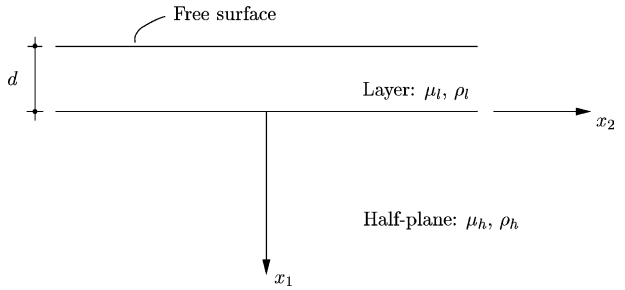

Fig. 7. Layer with a free surface supported on a half-plane; this geometry admits Love-wave motion.

3.2. Perfectly matched medium

The summation convention is abandoned in this section.

Consider a system of equations of the same form as Eq. (36), but with x_i replaced by stretched coordinates $\tilde{x}_i$, defined as [34]

$$\tilde{x}_i := \int_0^{x_i} \lambda_i(s)\,\mathrm{d}s, \tag{40}$$

where λ_i are nowhere-zero, continuous, complex-valued coordinate stretching functions. This coordinate stretching formally implies

$$\frac{\partial}{\partial \tilde{x}_i} = \frac{1}{\lambda_i(x_i)}\frac{\partial}{\partial x_i}; \tag{41}$$

thus, this system of equations can be defined as

$$\sum_i \frac{1}{\lambda_i(x_i)}\frac{\partial \sigma_i}{\partial x_i} = -\omega^2 \rho u, \tag{42a}$$

$$\sigma_i = \mu \varepsilon_i, \tag{42b}$$

$$\varepsilon_i = \frac{1}{\lambda_i(x_i)}\frac{\partial u}{\partial x_i}, \tag{42c}$$

as a modification of Eq. (36), where the constitutive relation (Eq. (42b)) remains the same as for the elastic medium. A PMM for anti-plane motion of a two-dimensional elastic continuum is defined to be one governed by Eq. (42); a (visco)elastic medium corresponds to $\lambda_i(x_i) \equiv 1$. Eq. (42) is defined independently of, but motivated by, the definition of $\tilde{x}_i$; this is comparable to the definition of Eq. (9) for the one-dimensional PMM.

Given the continuity of λ_i, solutions admitted in the PMM are similar in form to those in Eqs. (37) and (38) admitted in the elastic medium, but with x_i replaced by $\tilde{x}_i$. On an unbounded domain, Eq. (42) admits plane-wave-type solutions of the form

$$u(\boldsymbol{x}) = \exp[-\mathrm{i}k_{\mathrm{s}}\tilde{\boldsymbol{x}} \cdot \boldsymbol{p}]. \tag{43}$$

Furthermore, on the domain shown in Fig. 7 and given $\lambda_1(x_1) \equiv 1$, Eq. (42) admits Love-wave-type solutions of the form

$$u(\boldsymbol{x}) = (B_1 \mathrm{e}^{-\mathrm{i}\beta_l x_1} + B_2 \mathrm{e}^{+\mathrm{i}\beta_l x_1})\,\mathrm{e}^{-\mathrm{i}k_{\mathrm{v}}\tilde{x}_2} \quad \text{in the layer,} \tag{44a}$$

$$u(\boldsymbol{x}) = B_3\, \mathrm{e}^{-\beta_h x_1} \mathrm{e}^{-\mathrm{i}k_\mathrm{v}\tilde{x}_2} \quad \text{in the half-plane,} \tag{44b}$$

with β_l, β_h, k_v etc., as defined for the elastic medium.

The perfect matching property of these PMMs is that if two PMMs with different λ_i are placed adjacent to each other, with the functions λ_i for the two media such that they match at the interface of the media, then a propagating wave will pass through the interface without generating any reflected wave. This property is shown as follows. It is implicitly assumed in the definition of the PMM that λ_i is a function of x_i only, i.e., the coordinate stretches are uncoupled [34]. Consider the x_1–x_2 plane, with two PMMs defined on it: one on the left half plane ($:= \{(x_1,x_2)|x_1 < 0\}$) with $\lambda_i(x_i) := \lambda_i^{\mathrm{lt}}(x_i)$, and another on the right half plane ($:= \{(x_1,x_2)|x_1 \geqslant 0\}$) with $\lambda_i(x_i) := \lambda_i^{\mathrm{rt}}(x_i)$. If $\lambda_2^{\mathrm{lt}} = \lambda_2^{\mathrm{rt}}$, and if $\lambda_1^{\mathrm{lt}}(0) = \lambda_1^{\mathrm{rt}}(0)$, then the two PMMs can be considered as one PMM, wherein a continuous λ_1 is defined piecewise on the two half planes, and each λ_i is a function of x_i only; thus there is no interface to generate any reflected wave. This Perfect matching property holds for any wave solution admitted by the PMM. In particular, for a plane-wave-type solution as in Eq. (43), the matching is independent of the direction of propagation $\boldsymbol{p}$ and of the wave number k_s (or frequency ω).

A suitable choice of λ_i imposes an attenuation on the wave solutions to Eq. (42). Consider the plane wave-type solution in Eq. (43). If the functions λ_i are defined in terms of real-valued, continuous attenuation functions f_i as

$$\lambda_i(x_i) := 1 - \mathrm{i}\frac{f_i(x_i)}{k_\mathrm{s}}, \tag{45}$$

then

$$\tilde{x}_i = x_i - \mathrm{i}\frac{F_i(x_i)}{k_\mathrm{s}}, \tag{46}$$

where

$$F_i(x_i) := \int_0^{x_i} f_i(\xi)\,\mathrm{d}\xi. \tag{47}$$

Substituting Eq. (46) into Eq. (43) gives

$$u(\boldsymbol{x}) = \exp\left[-\sum_i F_i(x_i)p_i\right] \exp[-\mathrm{i}k_\mathrm{s}\boldsymbol{x}\cdot\boldsymbol{p}]. \tag{48}$$

Thus, if $F_i(x_i) > 0$ and $p_i > 0$, then $u(\boldsymbol{x})$ is attenuated as $\exp[-F_i(x_i)p_i]$ in the x_i-direction, and the attenuation is independent of the frequency if p_i is. Furthermore, consider the Love-wave-type solution in Eq. (44); if λ_2 for the layer and for the half-plane are chosen as in Eq. (45), as

$$\lambda_2^l(x_2) := 1 - \mathrm{i}\frac{f_2(x_2)}{k_\mathrm{s}^l} \tag{49a}$$

in the layer, and

$$\lambda_2^h(x_2) := 1 - \mathrm{i}\frac{f_2(x_2)}{k_\mathrm{s}^h} \tag{49b}$$

in the half-plane, then the $\exp(-\mathrm{i}k_\mathrm{v}\tilde{x}_2)$ term in Eq. (44), which represents a wave propagating in the positive x_2-direction, is transformed to

$$\exp\left[-F_2(x_2)\frac{c_\mathrm{s}^l}{c_\mathrm{v}}\right]\mathrm{e}^{-\mathrm{i}k_\mathrm{v}x_2}$$

in the layer, and to

$$\exp\left[-F_2(x_2)\frac{c_s^h}{c_v}\right]e^{-ik_v x_2}$$

in the half-plane. Since c_v depends on ω through Eq. (39), the attenuation is not independent of frequency for the choices of λ_2 given above. The use of k_v in place of k_s^l and k_s^h in Eq. (49) would, of course, make the attenuation independent of frequency, but would require the solution of Eq. (39) to determine k_v.

In a PMM for viscoelastic medium, with damping incorporated through the correspondence principle, the complex wave number k_s^* may be used in place k_s throughout, even in the stretching function, e.g., in Eq. (45).

3.3. Perfectly matched layer

Consider a wave of the form in Eq. (37) propagating in an unbounded elastic domain, the x_1–x_2 plane, governed by Eq. (36). The objective of defining a PML is to simulate this wave propagation by using a corresponding bounded domain. Consider the replacement of the unbounded domain by $\Omega_{BD} \cup \Omega_{PM}^{\infty}$ as shown in Fig. 8(a), where Ω_{BD} is a "bounded" (truncated) domain, governed by Eq. (36), and Ω_{PM}^{∞} is the unbounded PMM, governed by Eq. (42), with λ_1 of the form in Eq. (45), satisfying $f_1(0) = 0$, and $\lambda_2 \equiv 1$. Because a) the medium in Ω_{BD} is a special PMM ($\lambda_i(x_i) \equiv 1$, no summation), and b) the functions λ_i for the two media are chosen to be matched at the interface, all waves of the form in Eq. (37) propagating outwards from Ω_{BD} (waves with $p_1 > 0$) are completely absorbed into and then attenuated in the x_1-direction in Ω_{PM}^{∞}. Thus the displacements in Ω_{BD} due to an outward propagating wave are exactly the same as the displacements of the original unbounded elastic medium in Ω_{BD} due to the same wave.

If this outward propagating wave is attenuated enough in a finite distance, then Ω_{PM}^{∞} can be truncated by a fixed boundary without any significant reflection of the wave. Shown in Fig. 8(b), this layer Ω_{PM} of the PMM is termed the PML. If the wave reflection from the fixed boundary is not significant, then the displacements of this system ($\Omega_{BD} \cup \Omega_{PM}$) in Ω_{BD} should be almost the same as those of the unbounded elastic

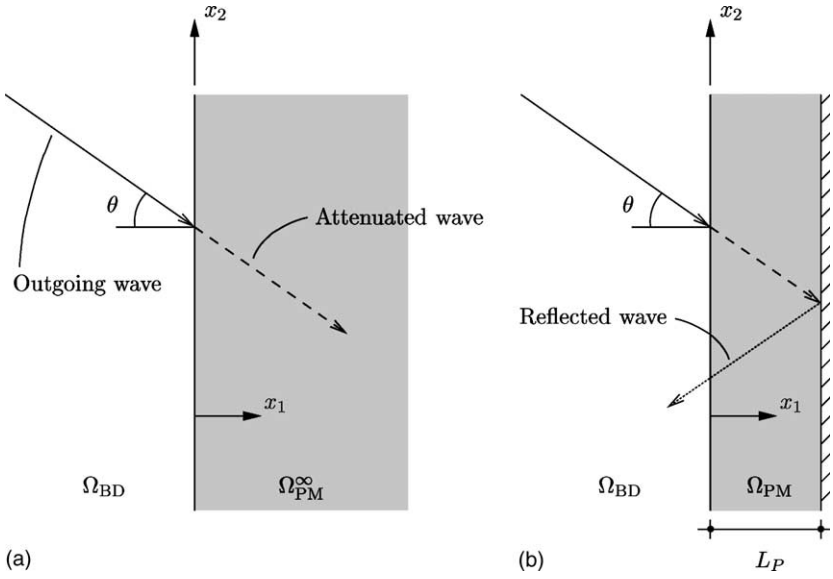

Fig. 8. (a) A PMM adjacent to a "bounded" (truncated) domain attenuates an outgoing plane wave; (b) a PML with a fixed edge also reflects the wave back towards the bounded domain.

domain in Ω_{BD}. A PML for the system shown in Fig. 7 can be constructed similarly by using a vertical layer consisting of two different PMMs with material properties matched to the physical layer and the half-plane.

The effect of domain truncation in the PMM is analysed by studying the reflection of plane waves by the fixed boundary. As shown in Fig. 8(b), the plane wave, incident at an angle θ and of unit amplitude as it enters the PML, is reflected from the fixed boundary. Therefore, the total wave motion can be represented as

$$u(\boldsymbol{x}) = \exp[-\mathrm{i}k_{\mathrm{s}}\tilde{\boldsymbol{x}}\cdot\boldsymbol{p}^{(\mathrm{I})}] + R\exp[-\mathrm{i}k_{\mathrm{s}}\tilde{\boldsymbol{x}}\cdot\boldsymbol{p}^{(\mathrm{R})}], \tag{50}$$

where $\boldsymbol{p}^{(\mathrm{I})}$ and $\boldsymbol{p}^{(\mathrm{R})}$ are the propagation directions of the incident and reflected waves respectively. Imposing $u(\boldsymbol{x}) \equiv 0$ for $x_1 = L_P$ and for all x_2, and substituting $p_1^{(\mathrm{I})} = \cos\theta$, gives

$$|R| = \exp[-2F_1(L_P)\cos\theta], \tag{51}$$

which is also the amplitude of the reflected wave as it exits the PML. This reflection coefficient is controlled by the choice of the parameters f_1 and L_P—independently of the size of the bounded domain to which the PML is adjacent—and is influenced by the angle of incidence. This suggests that the bounded domain may be restricted to the region of interest in the analysis, thus lowering the computational cost, if the parameters and the orientation of the PML are chosen appropriately.

3.4. An alternate interpretation of the PMM

Below is an equivalent interpretation of the anti-plane PMM as an anisotropic, inhomogeneous viscoelastic medium, obtained by transforming the coordinate stretch into a change in the constitutive relation. Consider two rectangular Cartesian coordinate systems for the plane as follows: (1) an x_i system, with respect to an orthonormal basis $\{\boldsymbol{e}_i\}$, and (2) an x_i' system, with respect to another orthonormal basis $\{\boldsymbol{e}_i'\}$, with the two bases related by the rotation-of-basis matrix $\mathbf{Q}$, with components $Q_{ij} := \boldsymbol{e}_i \cdot \boldsymbol{e}_j'$. Eq. (42) can be re-written in terms of the coordinates x_i' by replacing x_i by x_i' throughout, as (no summation)

$$\sum_i \frac{1}{\lambda_i(x_i')}\frac{\partial\sigma_i'}{\partial x_i'} = -\omega^2\rho u, \tag{52a}$$

$$\sigma_i' = \mu\varepsilon_i', \tag{52b}$$

$$\varepsilon_i' = \frac{1}{\lambda_i(x_i')}\frac{\partial u}{\partial x_i'}, \tag{52c}$$

representing a PMM wherein waves are attenuated in the $\boldsymbol{e}_1'$ and $\boldsymbol{e}_2'$ directions instead of in the $\boldsymbol{e}_1$ and $\boldsymbol{e}_2$ directions as in Eq. (42); σ_i' and ε_i' are the $3i$ components in the basis $\{\boldsymbol{e}_i'\}$ of the stress and strain tensors. By multiplying Eq. (52a) with $\lambda_1(x_1')\lambda_2(x_2')$ and using the fact that λ_i is a function of x_i' only, Eq. (52) can be re-written as

$$\boldsymbol{\nabla}'\cdot(\widetilde{\boldsymbol{\Lambda}}'\boldsymbol{\sigma}') = -\omega^2\rho[\lambda_1(x_1')\lambda_2(x_2')]u, \tag{53a}$$

$$\boldsymbol{\sigma}' = \mu\boldsymbol{\varepsilon}', \tag{53b}$$

$$\boldsymbol{\varepsilon}' = \boldsymbol{\Lambda}'(\boldsymbol{\nabla}'u), \tag{53c}$$

where

$$\boldsymbol{\sigma}' := \begin{Bmatrix}\sigma_1'\\ \sigma_2'\end{Bmatrix}, \quad \boldsymbol{\varepsilon}' := \begin{Bmatrix}\varepsilon_1'\\ \varepsilon_2'\end{Bmatrix}, \quad \boldsymbol{\nabla}' := \begin{Bmatrix}\dfrac{\partial}{\partial x_1'}\\ \dfrac{\partial}{\partial x_2'}\end{Bmatrix}, \tag{54}$$

and

$$\widetilde{\mathbf{\Lambda}}' := \begin{bmatrix} \lambda_2(x_2') & \cdot \\ \cdot & \lambda_1(x_1') \end{bmatrix}, \quad \mathbf{\Lambda}' := \begin{bmatrix} 1/\lambda_1(x_1') & \cdot \\ \cdot & 1/\lambda_2(x_2') \end{bmatrix}. \tag{55}$$

The various primed quantities in Eq. (53) can be transformed to the basis $\{\boldsymbol{e}_i'\}$ to obtain

$$\boldsymbol{\nabla} \cdot (\widetilde{\mathbf{\Lambda}}\boldsymbol{\sigma}) = -\omega^2 \rho [\lambda_1(x_1')\lambda_2(x_2')] u, \tag{56a}$$

$$\boldsymbol{\sigma} = \mu \boldsymbol{\varepsilon}, \tag{56b}$$

$$\boldsymbol{\varepsilon} = \mathbf{\Lambda}(\boldsymbol{\nabla} u), \tag{56c}$$

where

$$\boldsymbol{\sigma} := \begin{Bmatrix} \sigma_1 \\ \sigma_2 \end{Bmatrix} = \mathbf{Q}\boldsymbol{\sigma}', \quad \boldsymbol{\varepsilon} := \begin{Bmatrix} \varepsilon_1 \\ \varepsilon_2 \end{Bmatrix} = \mathbf{Q}\boldsymbol{\varepsilon}', \quad \boldsymbol{\nabla} := \begin{Bmatrix} \dfrac{\partial}{\partial x_1} \\ \dfrac{\partial}{\partial x_2} \end{Bmatrix} = \mathbf{Q}\boldsymbol{\nabla}', \tag{57}$$

and

$$\widetilde{\mathbf{\Lambda}} = \mathbf{Q}\widetilde{\mathbf{\Lambda}}'\mathbf{Q}^{\mathrm{T}}, \qquad \mathbf{\Lambda} = \mathbf{Q}\mathbf{\Lambda}'\mathbf{Q}^{\mathrm{T}}; \tag{58}$$

the tensors $\widetilde{\mathbf{\Lambda}}$ and $\mathbf{\Lambda}$ are termed the *left* and *right stretch tensors*, respectively. Furthermore, because these stretch tensors are diagonal in the basis $\{\boldsymbol{e}_i'\}$, this basis is termed the *characteristic basis* of the PMM. Redefining $\boldsymbol{\sigma}$ as $\boldsymbol{\sigma} \leftarrow \widetilde{\mathbf{\Lambda}}\boldsymbol{\sigma}$ and $\boldsymbol{\varepsilon}$ as $\boldsymbol{\varepsilon} \leftarrow \mathbf{\Lambda}^{-1}\boldsymbol{\varepsilon}$ in Eq. (56), and defining

$$f_{\mathrm{m}} := \lambda_1(x_1')\lambda_2(x_2') \tag{59}$$

gives an equivalent system of equations:

$$\boldsymbol{\nabla} \cdot \boldsymbol{\sigma} = -\omega^2 \rho f_{\mathrm{m}} u, \tag{60a}$$

$$\boldsymbol{\sigma} = \mu \mathbf{D} \boldsymbol{\varepsilon}, \tag{60b}$$

$$\boldsymbol{\varepsilon} = \boldsymbol{\nabla} u, \tag{60c}$$

where

$$\mathbf{D} := \widetilde{\mathbf{\Lambda}}\mathbf{\Lambda} = \mathbf{Q}\widetilde{\mathbf{\Lambda}}'\mathbf{\Lambda}'\mathbf{Q}^{\mathrm{T}}. \tag{61}$$

The coordinate-stretching in the PMM, represented by $\widetilde{\mathbf{\Lambda}}$ and $\mathbf{\Lambda}$ in Eq. (56), has thus been transformed into a change in the constitutive relation, thus leading to an interpretation of this PMM as an anisotropic, inhomogeneous viscoelastic medium. This interpretation of the PMM is comparable to the inhomogeneous-media interpretation of the one-dimensional PMM presented earlier and is also related to similar interpretations of electromagnetics PMLs [35,40].

3.5. Finite-element implementation

Next, the anisotropic, inhomogeneous medium form of the PMM, given by Eq. (60), is implemented using standard displacement-based finite elements. The weak form of Eq. (60a) is derived by multiplying it with an arbitrary weighting function w residing in an appropriate admissible space, and then integrating over the entire computational domain Ω using integration-by-parts and the divergence theorem to obtain

$$\int_{\Omega} \boldsymbol{\nabla} w \cdot \boldsymbol{\sigma} \, \mathrm{d}\Omega - \omega^2 \int_{\Omega} \rho f_{\mathrm{m}} w u \, \mathrm{d}\Omega = \int_{\Gamma} w \boldsymbol{\sigma} \cdot \boldsymbol{n} \, \mathrm{d}\Gamma, \tag{62}$$

where $\Gamma := \partial\Omega$ is the boundary of Ω and $\boldsymbol{n}$ is the unit normal to Γ. Assuming elementwise interpolations of u and w in terms of nodal shape functions $\boldsymbol{N}$, imposing Eqs. (60b) and (60c) pointwise in Eq. (62), and

restricting the domain integrals to the element domain $\Omega = \Omega^{\mathrm{e}}$ gives the stiffness and mass matrices for a PML element. In terms of nodal submatrices, these are

$$\mathbf{k}^{\mathrm{e}}_{IJ} = \int_{\Omega^{\mathrm{e}}} (\mathbf{\nabla} N_I)^{\mathrm{T}} \mu \mathbf{D} (\mathbf{\nabla} N_J)\, \mathrm{d}\Omega, \tag{63a}$$

$$\mathbf{m}^{\mathrm{e}}_{IJ} = \int_{\Omega^{\mathrm{e}}} \rho f_{\mathrm{m}} N_I N_J\, \mathrm{d}\Omega, \tag{63b}$$

where I and J denote node numbers of the element. In Eq. (63), the functions λ_i in $\mathbf{D}$ and in f_{m} are defined globally on the computational domain, not elementwise. Note that a FE implementation of Eq. (56) would also have resulted in the stiffness and mass matrices in Eq. (63), because the coordinate-stretch model of the PMM (Eq. (56)) is equivalent to the anisotropic-medium model (Eq. (60)).

The above is, of course, the FE implementation presented by Collino and Monk [41] and studied further by Harari et al. [25]. These element matrices are symmetric, but intrinsically complex-valued and frequency-dependent. Hence, the system matrices for Ω will be complex, symmetric, and banded, the PML contributions to which will have to computed anew for each frequency.

3.6. Numerical results

Consider a homogeneous isotropic semi-infinite layer of depth d on a rigid base, as shown in Fig. 9(a), whose anti-plane motion is governed by Eq. (36) with the following boundary conditions:

$$u(\boldsymbol{x}) = 0 \quad \text{at } x_2 = 0, \ \forall x_1 > 0, \tag{64a}$$

$$\sigma_2 = 0 \quad \text{at } x_2 = d, \ \forall x_1 > 0, \tag{64b}$$

$$u(\boldsymbol{x}) = u_1 N_1(x_2/d) + u_2 N_2(x_2/d) \quad \text{at } x_1 = 0, \ \forall x_2 \in [0, d], \tag{64c}$$

and a radiation condition for $x_1 \to \infty$, where u_1 and u_2 are the displacements at nodes 1 and 2 and N_1 and N_2 are shape functions, defined as

$$N_1(\xi) = 4\xi(1-\xi), \quad N_2(\xi) = \xi(2\xi - 1), \quad \xi \in [0, 1]. \tag{65}$$

The wave motion in this waveguide system is similar to Love-wave motion: it is dispersive, and consists of not only propagating modes but also an infinite number of evanescent modes, with the propagation (and decay) in the x_1-direction [42, Appendix A.3].

The nodal forces P_1 and P_2 at nodes 1 and 2 are related to the nodal displacements through the dynamic stiffness matrix $\mathbf{S}^{\infty}(a_0)$ as

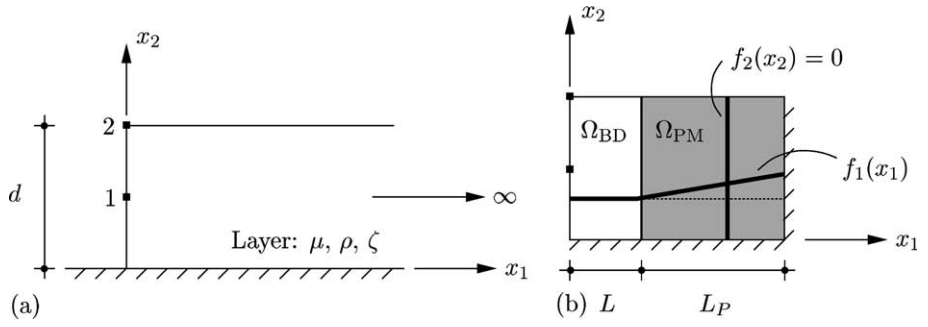

Fig. 9. (a) Homogeneous isotropic (visco)elastic semi-infinite layer of depth d on a fixed base; (b) a PML model.

$$\begin{Bmatrix} P_1 \\ P_2 \end{Bmatrix} = \mathbf{S}^{\infty}(a_0) \begin{Bmatrix} u_1 \\ u_2 \end{Bmatrix}, \tag{66}$$

where

$$\mathbf{S}^{\infty}(a_0) = 2\mu \sum_{n=0}^{\infty} \frac{\sqrt{\alpha_n^2 - a_0^2}}{\alpha_n^4} \begin{bmatrix} (-4 + (-1)^n 8/\alpha_n)^2 & -12 + (-1)^n 40/\alpha_n - 32/\alpha_n^2 \\ -12 + (-1)^n 40/\alpha_n - 32/\alpha_n^2 & (3 - (-1)^n 4/\alpha_n)^2 \end{bmatrix}, \tag{67}$$

with $a_0 = k_s d$ and $\alpha_n = (2n+1)\pi/2$. Furthermore, the components $S_{ij}(a_0)$ of $\mathbf{S}^{\infty}(a_0)$ can be decomposed into dimensionless, frequency-dependent stiffness, $k(a_0)$, and damping, $c(a_0)$, coefficients as

$$S_{ij}(a_0) = S_{ij}(0)[k_{ij}(a_0) + \mathrm{i} a_0 c_{ij}(a_0)] \text{ (no summation)}. \tag{68}$$

This semi-infinite layer is modelled using the bounded-domain-PML model shown in Fig. 9(b), composed of a bounded domain Ω_{BD} and a PML Ω_{PM}. Motivated by the realistic choice of a stretching function in Eq. (18), the stretching functions λ_i are chosen as

$$\lambda_i(x_i) := \left[1 + \frac{f_i(x_i)}{k_s^*}\right] - \mathrm{i}\frac{f_i(x_i)}{k_s^*} \tag{69}$$

to attenuate both propagating and evanescent waves in the system, with f_1 chosen to be linear in the PML—in view of the conclusions of Section 2.5—and $f_2 = 0$ matching the corresponding function in Ω_{BD}; recall that $k_s^* = k_s$ for an elastic medium. However, a stretching function of the form

$$\lambda_i(x_i) := [1 + f_i(x_i)] - \mathrm{i}\frac{f_i(x_i)}{k_s} \tag{70}$$

will not be adequate for all evanescent modes, an observation mirrored in electromagnetics literature [43,44], where alternative choices of the stretching function have been suggested for attenuating evanescent waves.

A uniform FE mesh of four-node bilinear isoparametric elements is used to discretise the entire bounded domain. The mesh is chosen to have n_d elements per unit d, n_b elements per unit L/d across the width of Ω_{BD}, and n_p elements per unit L_P/d across Ω_{PM}, where n_d, n_b and n_p are parameters in the analysis.

Figs. 10 and 11 show the effect of mesh density in the PML on the accuracy of the dynamic stiffness for two different values of n_b. Note that a denser mesh in the PML does not affect the results for low frequencies and, in fact, may lead to a deterioration in accuracy for higher frequencies. This suggests that the mesh density in the PML should be chosen to be similar to that in the bounded domain, echoing conclusions reached by an earlier dispersion analysis [25].

For purposes of comparison, the layer is also modelled using a viscous dashpot model [10], with consistent dashpots placed at the edge $x_1 = L + L_P$, and the entire domain $\Omega_{\mathrm{BD}} \cup \Omega_{\mathrm{PM}}$ taken to be elastic. The placement of the viscous dashpots is such that the mesh is comparable to that in the PML model. Fig. 12 presents stiffness and damping coefficients calculated for an elastic medium using the PML model and the viscous dashpot model. It is seen that the results from the PML model are highly accurate, even though they are obtained using a small computational domain and at a low cost: the cost of the PML model is similar to that of the viscous dashpot model, and the grossly inaccurate results from the viscous dashpot model emphasize the small size of the computational domain. Significantly, the high accuracy of the PML results demonstrates that the stretching function of Eq. (69) adequately attenuates the infinite number of evanescent modes in this waveguide.

Fig. 13 shows that the PML model gives highly accurate results for a viscoelastic medium with $\zeta = 0.05$. The appreciable inaccuracy in the results from the viscous dashpot model, even for this viscoelastic medium, further emphasizes the small size of the computational domain.

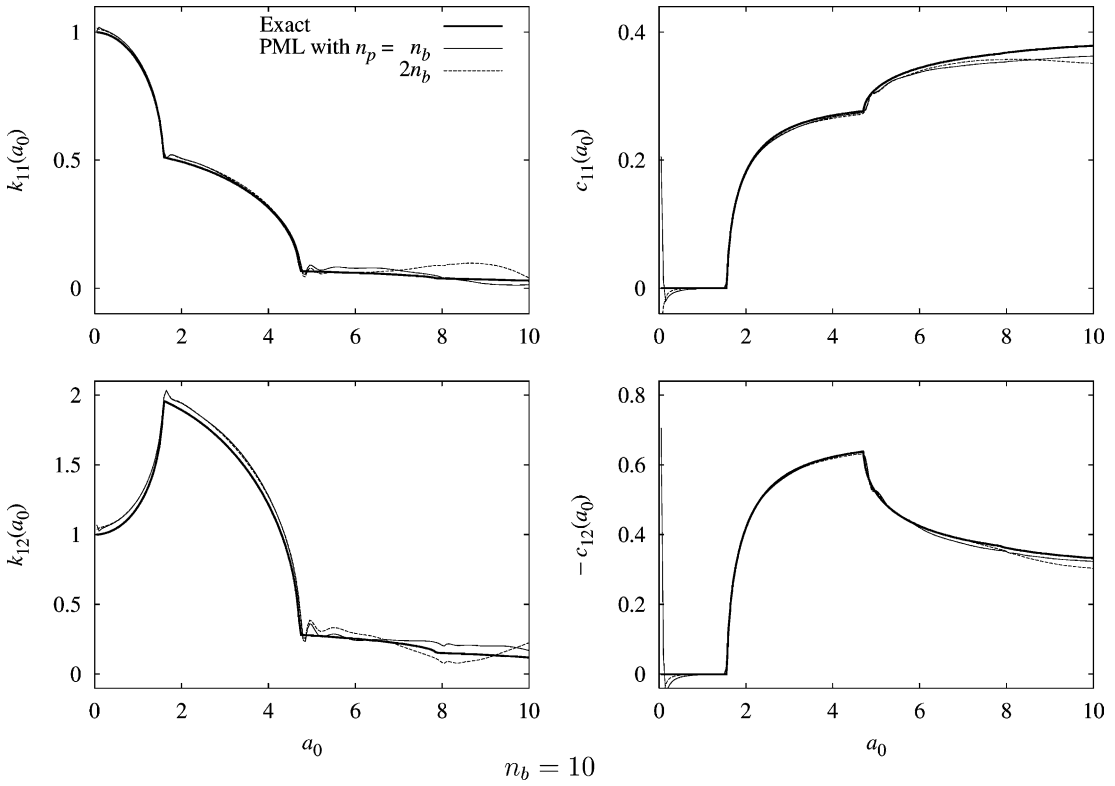

Fig. 10. Effect of mesh density in the PML on accuracy of dynamic stiffness of elastic semi-infinite layer on fixed base; $L = d/2$, $L_P = d$, $n_d = 15$, $f_1(x_1) = 10\langle x_1 - L\rangle/L_P$; $\langle x\rangle := (x + |x|)/2$.

4. Plane-strain and three-dimensional motion

4.1. Elastic medium

Consider a homogeneous isotropic elastic medium undergoing time-harmonic motion in the absence of body forces, with displacements of the form $\boldsymbol{u}(\boldsymbol{x})\exp(\mathrm{i}\omega t)$, where ω the excitation frequency. Such a medium is governed by the equations

$$\sum_j \frac{\partial \sigma_{ij}}{\partial x_j} = -\omega^2 \rho u_i, \tag{71a}$$

$$\sigma_{ij} = \sum_{k,l} \mathsf{C}_{ijkl}\varepsilon_{kl}, \tag{71b}$$

$$\varepsilon_{ij} = \frac{1}{2}\left[\frac{\partial u_i}{\partial x_j} + \frac{\partial u_j}{\partial x_i}\right], \tag{71c}$$

where C_{ijkl} written in terms of the Kronecker delta δ_{ij} is

$$\mathsf{C}_{ijkl} = \left(\kappa - \frac{2}{3}\mu\right)\delta_{ij}\delta_{kl} + \mu(\delta_{ik}\delta_{jl} + \delta_{il}\delta_{jk}), \tag{72}$$

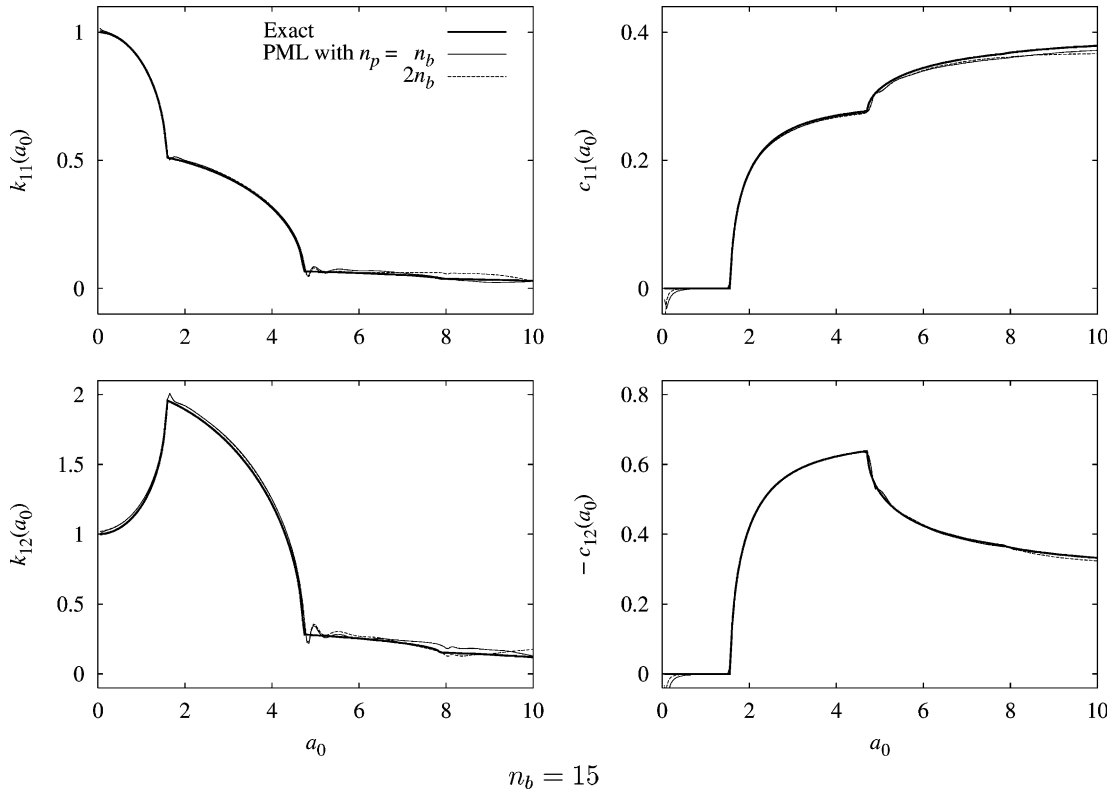

Fig. 11. Effect of mesh density in the PML on accuracy of dynamic stiffness of elastic semi-infinite layer on fixed base; $L = d/2$, $L_P = d$, $n_d = 15$, $f_1(x_1) = 10\langle x_1 - L\rangle/L_P$.

σ_{ij} and ε_{ij} are the components of $\boldsymbol{\sigma}$ and $\boldsymbol{\varepsilon}$, the stress and infinitesimal strain tensors, and C_{ijkl} are the components of $\mathbf{C}$, the material stiffness tensor; κ is the bulk modulus, μ the shear modulus, and ρ the mass density of the medium. If $i,j,k,l \in \{1,2\}$, then Eq. (71) describes plane-strain motion; if $i,j,k,l \in \{1,2,3\}$ it describes three-dimensional motion. Eq. (71) also describes plane-stress motion, with $i,j,k,l \in \{1,2\}$, if κ is re-defined appropriately.

On an unbounded domain, Eq. (71) admits body-wave solutions [39] in the form of (1) P waves:

$$\boldsymbol{u}(\boldsymbol{x}) = \boldsymbol{q}\exp[-\mathrm{i}k_{\mathrm{p}}\boldsymbol{x}\cdot\boldsymbol{p}], \tag{73a}$$

where $k_{\mathrm{p}} = \omega/c_{\mathrm{p}}$, with $c_{\mathrm{p}} = \sqrt{(\kappa + 4\mu/3)/\rho}$ the P-wave speed, $\boldsymbol{p}$ is a unit vector denoting the propagation direction, and $\boldsymbol{q} = \pm\boldsymbol{p}$ the direction of particle motion, and (2) S waves:

$$\boldsymbol{u}(\boldsymbol{x}) = \boldsymbol{q}\exp[-\mathrm{i}k_{\mathrm{s}}\boldsymbol{x}\cdot\boldsymbol{p}], \tag{73b}$$

where $k_{\mathrm{s}} = \omega/c_{\mathrm{s}}$, with $c_{\mathrm{s}} = \sqrt{\mu/\rho}$ the S-wave speed, and $\boldsymbol{q}\cdot\boldsymbol{p} = 0$. Eq. (71) also admits interface-guided waves, such as Rayleigh waves and Stoneley waves. Rayleigh waves propagate along a free surface, and Stoneley waves may propagate along the interface of two semi-infinite elastic media. Both types of waves propagate with exponentially-decreasing amplitude in the direction normal to and away from the surface or interface, respectively.

A viscoelastic medium is described by the above equations, but with complex-valued moduli $\kappa^* = \kappa(1 + 2\mathrm{i}\zeta)$ and $\mu^* = \mu(1 + 2\mathrm{i}\zeta)$, with ζ the hysteretic damping ratio, and corresponding complex-valued wave speeds.

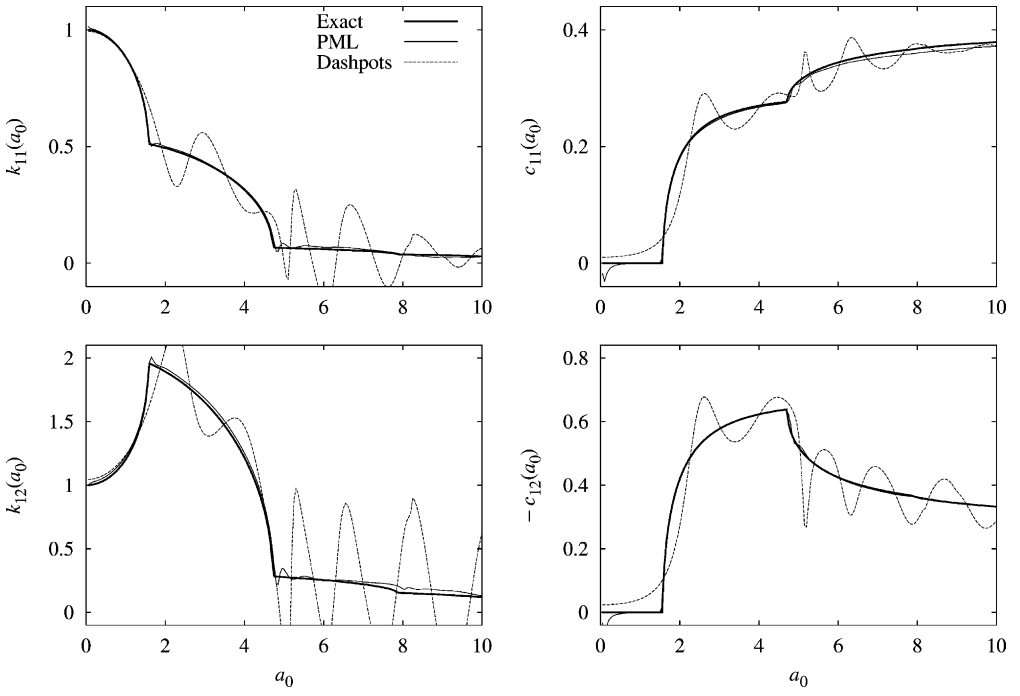

Fig. 12. Dynamic stiffness coefficients of elastic semi-infinite layer on fixed base computed using a PML model as well as a viscous dashpot boundary model; $L = d/2$, $L_P = d$, $n_b = n_p = 15$, $n_d = 15$, $f_1(x_1) = 10\langle x_1 - L\rangle/L_P$.

4.2. Perfectly matched medium and layer

The summation convention is abandoned in this section.

A PMM for plane-strain or three-dimensional elastodynamic motion is defined to be a medium governed by the following equations:

$$\sum_j \frac{1}{\lambda_j(x_j)} \frac{\partial \sigma_{ij}}{\partial x_j} = -\omega^2 \rho u_i, \tag{74a}$$

$$\sigma_{ij} = \sum_{k,l} \mathsf{C}_{ijkl} \varepsilon_{kl}, \tag{74b}$$

$$\varepsilon_{ij} = \frac{1}{2}\left[\frac{1}{\lambda_j(x_j)} \frac{\partial u_i}{\partial x_j} + \frac{1}{\lambda_i(x_i)} \frac{\partial u_j}{\partial x_i}\right], \tag{74c}$$

where λ_i are nowhere-zero, continuous, complex-valued coordinate stretching functions; the constitutive relation Eq. (74b) is the same as for the elastic medium. Consequently, Eq. (74) also describes a PMM for plane-stress motion, if κ is re-defined appropriately. A (visco)elastic medium corresponds to $\lambda_i(x_i) \equiv 1$. Eq. (74) is defined independently of, but motivated by, the definition of $\tilde{x}_i$ given by Eq. (40).

The continuity of λ_i can be used to show that on an unbounded domain, Eq. (74) admits solutions of the same form as Eq. (73), but with $\boldsymbol{x}$ replaced by $\tilde{\boldsymbol{x}}$. A P-type wave solution is of the form

$$\boldsymbol{u}(\boldsymbol{x}) = \boldsymbol{q} \exp[-\mathrm{i} k_{\mathrm{p}} \tilde{\boldsymbol{x}} \cdot \boldsymbol{p}], \tag{75a}$$

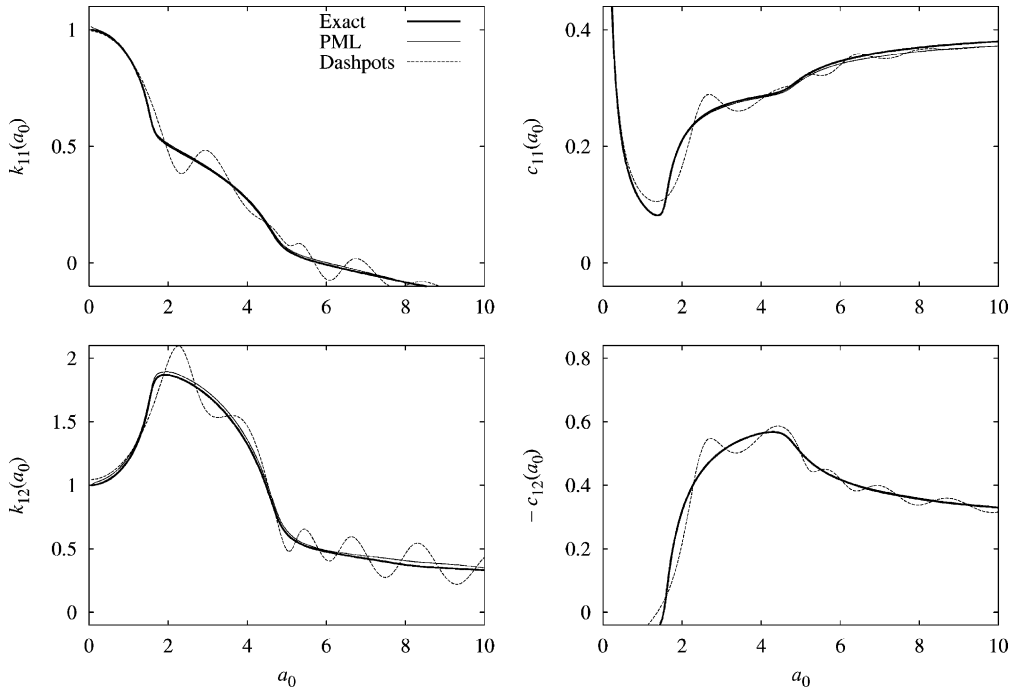

Fig. 13. Dynamic stiffness coefficients of viscoelastic semi-infinite layer on fixed base computed using a PML model as well as a viscous dashpot boundary model; $L = d/2$, $L_P = d$, $n_b = n_p = 15$, $n_d = 15$, $f_1(x_1) = 10\langle x_1 - L\rangle/L_P$; $\zeta = 0.05$.

with $\boldsymbol{q} = \pm\boldsymbol{p}$, and an S-type wave solution is of the form

$$\boldsymbol{u}(\boldsymbol{x}) = \boldsymbol{q}\exp[-\mathrm{i}k_{\mathrm{s}}\tilde{\boldsymbol{x}}\cdot\boldsymbol{p}], \tag{75b}$$

with $\boldsymbol{q}\cdot\boldsymbol{p} = 0$. It can be argued that for appropriately defined λ_i and appropriate boundary conditions, Eq. (74) also admits solutions of the forms of Rayleigh and Stoneley waves. This is similar to the earlier observation that a PMM for anti-plane motion admits solutions of the form of Love waves.

These PMMs exhibit the perfect matching property: if two PMMs with different λ_i are placed adjacent to each other, with the functions λ_i for the two media such that they match at the interface of the media, then any propagating waveform will pass through the interface without generating any reflected wave. The argument for this claim is the same as that for PMMs for anti-plane motion.

A choice of λ_i of the form in Eq. (45) leads to attenuated solutions of the form

$$\boldsymbol{u}(\boldsymbol{x}) = \exp\left[-\frac{c_{\mathrm{s}}}{c_{\mathrm{p}}}\sum_i F_i(x_i)p_i\right]\boldsymbol{q}\exp[-\mathrm{i}k_{\mathrm{p}}\boldsymbol{x}\cdot\boldsymbol{p}] \tag{76a}$$

for P-type waves and

$$\boldsymbol{u}(\boldsymbol{x}) = \exp\left[-\sum_i F_i(x_i)p_i\right]\boldsymbol{q}\exp[-\mathrm{i}k_{\mathrm{s}}\boldsymbol{x}\cdot\boldsymbol{p}] \tag{76b}$$

for S-type waves if $F_i(x_i) > 0$ and $p_i > 0$, with F_i defined in Eq. (47); the attenuation is independent of the frequency if p_i is. It can be argued that suitable choices of λ_i lead to Rayleigh-type (and Stoneley-type) wave solutions that are attenuated in the direction of their propagation.

The absorptive and attenuative properties of the PMM can be used to define an absorbing layer—the PML—adjacent to a bounded domain, e.g., as shown in Fig. 8(b). The argument for this claim is as for anti-plane motion.

The absorptive capability of such a layer is analysed by studying the reflection of plane waves from the fixed boundary. Consider plane-strain motion in the domain shown in Fig. 8(b), with Ω_{BD} governed by Eq. (71) and Ω_{PM} governed by Eq. (74), with λ_1 of the form in Eq. (45), satisfying $f_1(0) = 0$, and $\lambda_2 \equiv 1$. Furthermore, consider a P-wave with unit amplitude as it enters the PML at an angle of incidence θ. The incident wave will be reflected from the boundary as a P-type wave and an S-type wave, with the total wave motion represented as

$$\boldsymbol{u}(\boldsymbol{x}) = \boldsymbol{q}_{\mathrm{p}}^{(\mathrm{I})} \exp[-\mathrm{i}k_{\mathrm{p}}\tilde{\boldsymbol{x}} \cdot \boldsymbol{p}_{\mathrm{p}}^{(\mathrm{I})}] + R_{\mathrm{pp}}\boldsymbol{q}_{\mathrm{p}}^{(\mathrm{R})} \exp[-\mathrm{i}k_{\mathrm{p}}\tilde{\boldsymbol{x}} \cdot \boldsymbol{p}_{\mathrm{p}}^{(\mathrm{R})}] + R_{\mathrm{sp}}\boldsymbol{q}_{\mathrm{s}}^{(\mathrm{R})} \exp[-\mathrm{i}k_{\mathrm{s}}\tilde{\boldsymbol{x}} \cdot \boldsymbol{p}_{\mathrm{s}}^{(\mathrm{R})}], \tag{77}$$

where the s and p subscripts refer to S-type and P-type waves, respectively, and superscripts (I) and (R) refer to incident and reflected waves, respectively. Imposing $\boldsymbol{u}(\boldsymbol{x}) \equiv 0$ for $x_1 = L_P$ and for all x_2, and expressing the directions of propagation and of particle motion in terms of θ, gives

$$|R_{\mathrm{pp}}| = \frac{\cos(\theta + \theta_{\mathrm{s}})}{\cos(\theta - \theta_{\mathrm{s}})} \exp\left[-2\frac{c_{\mathrm{s}}}{c_{\mathrm{p}}} F_1(L_P) \cos\theta \right], \tag{78a}$$

$$|R_{\mathrm{sp}}| = \frac{\sin 2\theta}{\cos(\theta - \theta_{\mathrm{s}})} \exp\left[-F_1(L_P)\left(\frac{c_{\mathrm{s}}}{c_{\mathrm{p}}} \cos\theta + \cos\theta_{\mathrm{s}} \right) \right], \tag{78b}$$

with θ_{s} given by

$$\sin\theta_{\mathrm{s}} = \frac{c_{\mathrm{s}}}{c_{\mathrm{p}}} \sin\theta;$$

a similar analysis can be performed to determine the reflection coefficients due to an incident S-type wave. The amplitudes of the reflected P- and S-type waves as they exit the PML, given by $|R_{\mathrm{pp}}|$ and $|R_{\mathrm{sp}}|$, respectively, are controlled by the choice of parameters f_1 and L_P—independently of the size of the bounded domain to which the PML is adjacent—and are also influenced by the angle of incidence. This suggests that the bounded domain may be restricted to the region of interest in the analysis, thus lowering the computational cost, if the parameters and the orientation of the PML are chosen appropriately.

4.3. Finite-element implementation

Unlike the PMM for anti-plane motion, the PMM for plane-strain or three-dimensional motion is not amenable to interpretation as an anisotropic, inhomogeneous viscoelastic medium; however, a symmetric FE implementation of this PMM can still be obtained, by expressing the PMM equations in a tensorial form. The implementation of only the plane-strain PMM is presented here; the implementation of the three-dimensional PMM follows similarly.

Consider two rectangular Cartesian coordinate systems for the plane: (1) a x_i system, with respect to an orthonormal basis $\{\boldsymbol{e}_i\}$, and (2) a x'_i system, with respect to another orthonormal basis $\{\boldsymbol{e}'_i\}$, with the two bases related by the rotation-of-basis matrix $\mathbf{Q}$, with components $Q_{ij} := \boldsymbol{e}_i \cdot \boldsymbol{e}'_j$. Eq. (74) can be re-written in the basis $\{\boldsymbol{e}'_i\}$ as (no summation)

$$\sum_j \frac{1}{\lambda_j(x'_j)} \frac{\partial \sigma'_{ij}}{\partial x'_j} = -\omega^2 \rho u'_i, \tag{79a}$$

$$\sigma'_{ij} = \sum_{k,l} \mathsf{C}'_{ijkl}\varepsilon'_{kl}, \tag{79b}$$

$$\varepsilon'_{ij} = \frac{1}{2}\left[\frac{1}{\lambda_j(x'_j)}\frac{\partial u'_i}{\partial x'_j} + \frac{1}{\lambda_i(x'_i)}\frac{\partial u'_j}{\partial x'_i}\right], \tag{79c}$$

where the various primed quantities represent the components in the basis $\{\boldsymbol{e}'_i\}$ of the corresponding vector or tensor. This represents a PMM where waves are attenuated in the $\boldsymbol{e}'_1$ and $\boldsymbol{e}'_2$ directions. On multiplying Eq. (79a) with $\lambda_1(x'_1)\lambda_2(x'_2)$ and using the fact that λ_i is a function of x'_i only, Eq. (79) can be re-written in matrix notation as

$$(\boldsymbol{\sigma}'\widetilde{\boldsymbol{\Lambda}}')\boldsymbol{\nabla}' = -\omega^2\rho[\lambda_1(x'_1)\lambda_2(x'_2)]\boldsymbol{u}', \tag{80a}$$

$$\boldsymbol{\sigma}' = \mathbf{C}'\boldsymbol{\varepsilon}', \tag{80b}$$

$$\boldsymbol{\varepsilon}' = \tfrac{1}{2}[(\boldsymbol{u}'\boldsymbol{\nabla}'^{\mathrm{T}})\boldsymbol{\Lambda}' + \boldsymbol{\Lambda}'^{\mathrm{T}}(\boldsymbol{u}'\boldsymbol{\nabla}'^{\mathrm{T}})^{\mathrm{T}}], \tag{80c}$$

where

$$\boldsymbol{\sigma}' := \begin{bmatrix}\sigma'_{11} & \sigma'_{12}\\ \sigma'_{21} & \sigma'_{22}\end{bmatrix}, \quad \boldsymbol{\varepsilon}' := \begin{bmatrix}\varepsilon'_{11} & \varepsilon'_{12}\\ \varepsilon'_{21} & \varepsilon'_{22}\end{bmatrix}, \quad \boldsymbol{u}' := \begin{Bmatrix}u'_1\\ u'_2\end{Bmatrix}, \quad \boldsymbol{\nabla}' := \begin{Bmatrix}\dfrac{\partial}{\partial x'_1}\\ \dfrac{\partial}{\partial x'_2}\end{Bmatrix} \tag{81}$$

and

$$\widetilde{\boldsymbol{\Lambda}}' := \begin{bmatrix}\lambda_2(x'_2) & \cdot\\ \cdot & \lambda_1(x'_1)\end{bmatrix}, \qquad \boldsymbol{\Lambda}' := \begin{bmatrix}1/\lambda_1(x'_1) & \cdot\\ \cdot & 1/\lambda_2(x'_2)\end{bmatrix}; \tag{82}$$

Eq. (80b) is understood in indicial notation. Eq. (80) can be transformed to the basis $\{\boldsymbol{e}_i\}$ to obtain

$$(\boldsymbol{\sigma}\widetilde{\boldsymbol{\Lambda}})\boldsymbol{\nabla} = -\omega^2\rho[\lambda_1(x'_1)\lambda_2(x'_2)]\boldsymbol{u}, \tag{83a}$$

$$\boldsymbol{\sigma} = \mathbf{C}\boldsymbol{\varepsilon}, \tag{83b}$$

$$\boldsymbol{\varepsilon} = \tfrac{1}{2}[(\boldsymbol{u}\boldsymbol{\nabla}^{\mathrm{T}})\boldsymbol{\Lambda} + \boldsymbol{\Lambda}^{\mathrm{T}}(\boldsymbol{u}\boldsymbol{\nabla}^{\mathrm{T}})^{\mathrm{T}}], \tag{83c}$$

where the unprimed quantities, e.g.,

$$\boldsymbol{\sigma} := \begin{bmatrix}\sigma_{11} & \sigma_{12}\\ \sigma_{21} & \sigma_{22}\end{bmatrix}, \quad \boldsymbol{\varepsilon} := \begin{bmatrix}\varepsilon_{11} & \varepsilon_{12}\\ \varepsilon_{21} & \varepsilon_{22}\end{bmatrix}, \quad \boldsymbol{u} := \begin{Bmatrix}u_1\\ u_2\end{Bmatrix} \quad \text{and} \quad \boldsymbol{\nabla} := \begin{Bmatrix}\dfrac{\partial}{\partial x_1}\\ \dfrac{\partial}{\partial x_2}\end{Bmatrix} \tag{84}$$

are obtained from the corresponding primed quantities in Eq. (80) via the usual change-of-basis rules for vector and tensor components, e.g.,

$$\widetilde{\boldsymbol{\Lambda}} = \mathbf{Q}\widetilde{\boldsymbol{\Lambda}}'\mathbf{Q}^{\mathrm{T}} \quad \text{and} \quad \boldsymbol{\Lambda} = \mathbf{Q}\boldsymbol{\Lambda}'\mathbf{Q}^{\mathrm{T}}. \tag{85}$$

Note that the stretch tensors $\widetilde{\boldsymbol{\Lambda}}$ and $\boldsymbol{\Lambda}$ are diagonal in the characteristic basis $\{\boldsymbol{e}'_i\}$ of the PMM. In tensorial notation, Eq. (83) becomes

$$\mathrm{div}(\boldsymbol{\sigma}\widetilde{\boldsymbol{\Lambda}}) = -\omega^2\rho[\lambda_1(x'_1)\lambda_2(x'_2)]\boldsymbol{u}, \tag{86a}$$

$$\boldsymbol{\sigma} = \mathbf{C}\boldsymbol{\varepsilon}, \tag{86b}$$

$$\boldsymbol{\varepsilon} = \tfrac{1}{2}[(\operatorname{grad}\boldsymbol{u})\boldsymbol{\Lambda} + \boldsymbol{\Lambda}^{\mathrm{T}}(\operatorname{grad}\boldsymbol{u})^{\mathrm{T}}]. \tag{86c}$$

The weak form of Eq. (86a) is derived by taking its inner product with an arbitrary weighting function $\boldsymbol{w}$ residing in an appropriate admissible space, and integrating the resultant scalar over the entire computational domain Ω using integration-by-parts and the divergence theorem to obtain

$$\int_{\Omega} \tilde{\boldsymbol{\varepsilon}} : \boldsymbol{\sigma}\,\mathrm{d}\Omega - \omega^2 \int_{\Omega} \rho f_{\mathrm{m}} \boldsymbol{w}\cdot\boldsymbol{u}\,\mathrm{d}\Omega = \int_{\Gamma} \boldsymbol{w}\cdot\boldsymbol{\sigma}\widetilde{\boldsymbol{\Lambda}}\boldsymbol{n}\,\mathrm{d}\Gamma, \tag{87}$$

with $\Gamma := \partial\Omega$ the boundary of Ω and $\boldsymbol{n}$ the unit normal to it, and f_{m} defined by Eq. (59). The symmetry of $\boldsymbol{\sigma}$ has been used to obtain the first integral on the left hand side, with

$$\tilde{\boldsymbol{\varepsilon}} = \tfrac{1}{2}[(\operatorname{grad}\boldsymbol{w})\widetilde{\boldsymbol{\Lambda}} + \widetilde{\boldsymbol{\Lambda}}^{\mathrm{T}}(\operatorname{grad}\boldsymbol{w})^{\mathrm{T}}]. \tag{88}$$

Assuming elementwise interpolations of $\boldsymbol{u}$ and $\boldsymbol{w}$ in terms of shape functions $\boldsymbol{N}$, imposing Eqs. (86b) and (86c) pointwise in Eq. (87), and restricting the integrals to the element domain $\Omega = \Omega^{\mathrm{e}}$ gives the stiffness and mass matrices for a PML element. In terms of nodal submatrices, with I and J the node numbers, these are

$$\mathbf{k}^{\mathrm{e}}_{IJ} = \int_{\Omega^{\mathrm{e}}} \widetilde{\mathbf{B}}_I^{\mathrm{T}}\mathbf{D}\mathbf{B}_J\,\mathrm{d}\Omega, \tag{89a}$$

$$\mathbf{m}^{\mathrm{e}}_{IJ} = \int_{\Omega^{\mathrm{e}}} \rho f_{\mathrm{m}} N_I N_J\,\mathrm{d}\Omega\,\mathbf{I}, \tag{89b}$$

where $\mathbf{I}$ is the identity matrix of size 2×2, and

$$\mathbf{D} := \begin{bmatrix} \kappa+4\mu/3 & \kappa-2\mu/3 & \cdot \\ \kappa-2\mu/3 & \kappa+4\mu/3 & \cdot \\ \cdot & \cdot & \mu \end{bmatrix}, \quad \widetilde{\mathbf{B}}_I := \begin{bmatrix} N^{(1)}_{I1} & \cdot \\ \cdot & N^{(1)}_{I2} \\ N^{(1)}_{I2} & N^{(1)}_{I1} \end{bmatrix}, \quad \mathbf{B}_I := \begin{bmatrix} N^{(2)}_{I1} & \cdot \\ \cdot & N^{(2)}_{I2} \\ N^{(2)}_{I2} & N^{(2)}_{I1} \end{bmatrix}, \tag{90}$$

with

$$N^{(1)}_{Ii} := \widetilde{\Lambda}_{ij} N_{I,j} \quad \text{and} \quad N^{(2)}_{Ii} := \Lambda_{ij} N_{I,j}. \tag{91}$$

In Eq. (89), the functions λ_i in $\widetilde{\mathbf{B}}$, $\mathbf{B}$ and in f_{m} are defined globally on the computational domain, not elementwise. The right hand side in Eq. (87) can be ignored by assuming that the traction-like term $\boldsymbol{\sigma}\widetilde{\boldsymbol{\Lambda}}\boldsymbol{n} = 0$ on a free boundary of the PMM. Note the evidence of coordinate-stretching in the FE matrices in Eq. (89): the stretch tensors $\widetilde{\boldsymbol{\Lambda}}$ and $\boldsymbol{\Lambda}$ are incorporated in the nodal compatibility matrices $\widetilde{\mathbf{B}}_I$ and $\mathbf{B}_I$, not in the material moduli matrix $\mathbf{D}$ (Eq. (90)). As a corollary, this plane-strain FE formulation can be applied to plane-stress problems by re-defining κ appropriately.

It is argued that the stiffness matrix given by Eq. (89a) is indeed symmetric, by first deriving an alternate expression for the nodal submatrix $\mathbf{k}^{\mathrm{e}}_{IJ}$. Consider the first integrand on the left hand side of Eq. (87). By the minor symmetries of C_{ijkl},

$$\tilde{\boldsymbol{\varepsilon}} : \boldsymbol{\sigma} = \tilde{\varepsilon}_{ij}\sigma_{ij} = w_{i,j}\widetilde{\mathsf{C}}_{ijkl}u_{k,l}, \tag{92}$$

where

$$\widetilde{\mathsf{C}}_{ijkl} := \widetilde{\Lambda}_{jm}\mathsf{C}_{imkn}\Lambda_{ln} = \left(\kappa - \tfrac{2}{3}\mu\right)\widetilde{\Lambda}_{ij}\Lambda_{kl} + \mu(\delta_{ik}\widetilde{\Lambda}_{jn}\Lambda_{ln} + \widetilde{\Lambda}_{jk}\Lambda_{il}) \tag{93}$$

by Eq. (72). The functions w_i and u_k are interpolated as

$$w_i = N_I c^I_i \quad \text{and} \quad u_k = N_J d^J_k, \tag{94}$$

where d_k^J is the nodal displacement at node J in the direction $\boldsymbol{e}_k$, and c_i^I is an arbitrary quantity associated with the direction $\boldsymbol{e}_i$ at node I. Introducing these interpolations into Eq. (87) and restricting the integral to Ω_e gives the nodal stiffness submatrix in terms of its components as

$$(\mathbf{k}^{\mathrm{e}}_{IJ})_{ik} = \int_{\Omega^{\mathrm{e}}} N_{I,j}\widetilde{\mathsf{C}}_{ijkl}N_{J,l}\,\mathrm{d}\Omega. \tag{95}$$

The stiffness matrix is symmetric if $(\mathbf{k}^{\mathrm{e}}_{IJ})_{ik} = (\mathbf{k}^{\mathrm{e}}_{JI})_{ki}$, which holds if $\widetilde{\mathsf{C}}_{ijkl} = \tilde{\mathsf{C}}_{klij}$, i.e., if $\widetilde{\mathsf{C}}_{ijkl}$ has major symmetry.

It is argued that $\widetilde{\mathsf{C}}_{ijkl}$ given by Eq. (93) indeed has major symmetry. Because major symmetry is preserved by a change of basis, it suffices to consider diagonal stretch tensors

$$\widetilde{\boldsymbol{\Lambda}} := \begin{bmatrix} \lambda_2(x_2) & \cdot \\ \cdot & \lambda_1(x_1) \end{bmatrix} \quad \text{and} \quad \boldsymbol{\Lambda} := \begin{bmatrix} 1/\lambda_1(x_1) & \cdot \\ \cdot & 1/\lambda_2(x_2) \end{bmatrix} \tag{96}$$

corresponding to the characteristic basis of the PMM; the primes on the coordinates have been discarded in the interest of notational convenience. Major symmetry of a fourth order tensor with indices $ijkl$ can be shown by expressing it in matrix form through Voigt indexing, wherein a tensor index pair ij is mapped to a single Voigt index a. The rows of the Voigt-indexed matrix are taken to correspond to indices ij and the columns to kl, with both index pairs enumerated in the same order. Major symmetry of a fourth order tensor is then equivalent to the symmetry of this matrix. Under the Voigt indexing given by

Voigt index	a:	1	2	3	4
Tensor index	ij:	11	22	12	21

the various terms in the expression for $\widetilde{\mathsf{C}}_{ijkl}$ in Eq. (93) have the following matrix representations:

$$\widetilde{\boldsymbol{\Lambda}}_{ij}\boldsymbol{\Lambda}_{kl} \equiv \begin{bmatrix} \lambda_2/\lambda_1 & 1 & & \\ 1 & \lambda_1/\lambda_2 & & \\ & & 0 & \\ & & & 0 \end{bmatrix} \quad \delta_{ik}\widetilde{\boldsymbol{\Lambda}}_{jn}\boldsymbol{\Lambda}_{ln} \equiv \begin{bmatrix} \lambda_2/\lambda_1 & & & \\ & \lambda_1/\lambda_2 & & \\ & & \lambda_1/\lambda_2 & \\ & & & \lambda_2/\lambda_1 \end{bmatrix}$$

$$\text{and} \quad \widetilde{\boldsymbol{\Lambda}}_{jk}\boldsymbol{\Lambda}_{il} \equiv \begin{bmatrix} \lambda_2/\lambda_1 & & & \\ & \lambda_1/\lambda_2 & & \\ & & 0 & 1 \\ & & 1 & 0 \end{bmatrix}. \tag{97}$$

The symmetry of these matrices thus implies the symmetry of the stiffness matrix.

Thus, the FE matrices are symmetric, but intrinsically complex-valued and frequency-dependent. Hence, the system matrices for Ω will be complex, symmetric, and banded, the PML contributions to which will have to computed anew for each frequency.

4.4. Numerical results

Numerical results are presented for the classical plane-strain soil–structure interaction problems of a rigid strip-footing on a (1) half-plane, (2) layer on a half-plane, and (3) layer on a rigid base.

Fig. 14(a) shows a cross-section of a rigid strip-footing of half-width b with its three degrees-of-freedom identified—vertical (V), horizontal (H), and rocking (R)—supported by a homogeneous isotropic (visco)elastic half-plane with shear modulus μ, mass density ρ, Poisson's ratio ν, and hysterstic damping ratio ζ

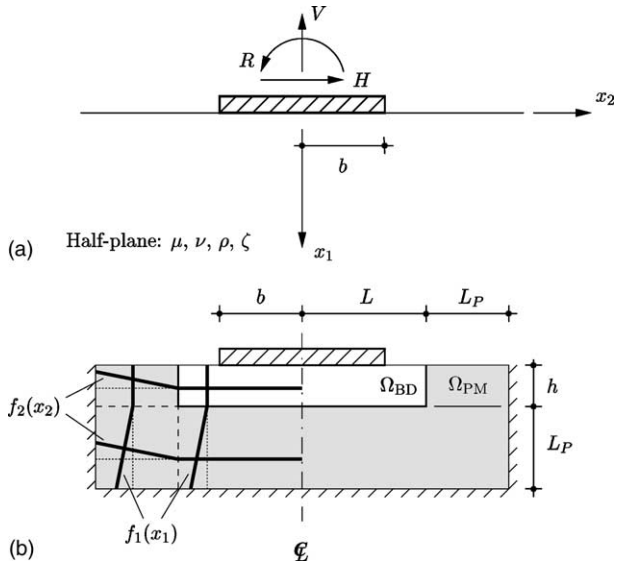

Fig. 14. (a) Cross-section of a rigid strip of half-width b on a homogeneous isotropic (visco)elastic half-plane; (b) a PML model.

for the viscoelastic medium. Let P_i and Δ_i, $i \in \{V, H, R\}$, denote the amplitudes of the harmonic force and of the harmonic displacement, respectively, along the ith DOF. The two are related through the dynamic flexibility matrix $\mathbf{F}^{\infty}(a_0)(a_0 = \omega b/c_s)$ as follows:

$$\begin{Bmatrix} \Delta_V \\ \Delta_H \\ b\Delta_R \end{Bmatrix} = \mathbf{F}^{\infty}(a_0) \begin{Bmatrix} P_V \\ P_H \\ P_R/b \end{Bmatrix} = \begin{bmatrix} F_{VV}(a_0) & 0 & 0 \\ 0 & F_{HH}(a_0) & F_{HR}(a_0) \\ 0 & F_{RH}(a_0) & F_{RR}(a_0) \end{bmatrix} \begin{Bmatrix} P_V \\ P_H \\ P_R/b \end{Bmatrix}. \tag{98}$$

This unbounded-domain system is modelled using the bounded-domain-PML model shown in Fig. 14(b), composed of a bounded domain Ω_{BD} and a PML Ω_{PM}. The stretching functions λ_i are chosen as in Eq. (69), with the attenuation functions chosen to be linear in the PML, following Section 2.5. Note that the choice of attenuation functions, especially in the corner regions, follows naturally from the requirements that $f_i \equiv 0$ in Ω_{BD}, f_i be a function of x_i only, and that f_i be continuous in the entire computational domain. A FE mesh of four-node bilinear isoparametric elements are used to discretise the entire bounded domain. The mesh is chosen to be adequately dense for the range of frequencies considered, and is graded to capture adequately sharp variations in stresses near the footing. For purposes of comparison, the half-space is also modelled using a viscous dashpot boundary model [9], wherein the entire domain $\Omega_{BD} \cup \Omega_{PM}$ is taken to be (visco)elastic and consistent viscous dashpot elements replace the fixed outer boundary. The mesh used for the dashpot model is thus comparable to that used for the PML model.

Fig. 15 presents the dynamic flexibility coefficients computed for an elastic medium from the PML model and from the dashpot model, against "exact" analytical results [45]. The domain size parameters are chosen to be $L = 3b/2$, $h = b/2$, $L_P = b$. Note that the bounded domain chosen is small, extending only upto $b/2$ on either side of the footing and below it, and the PML width equal to b, the half-width of the footing. Using this small domain, the results obtained from the PML model are highly accurate, even though they are obtained at a low computational cost: the cost of the PML model is similar to that of the viscous dashpot model. The gross inaccuracy of the results from the viscous dashpot model emphasizes the small size of the computational domain. Fig. 16 compares results for a viscoelastic medium with $\zeta = 0.05$, computed for the same meshes used for the elastic medium, with "exact" semi-analytical results [46]. The

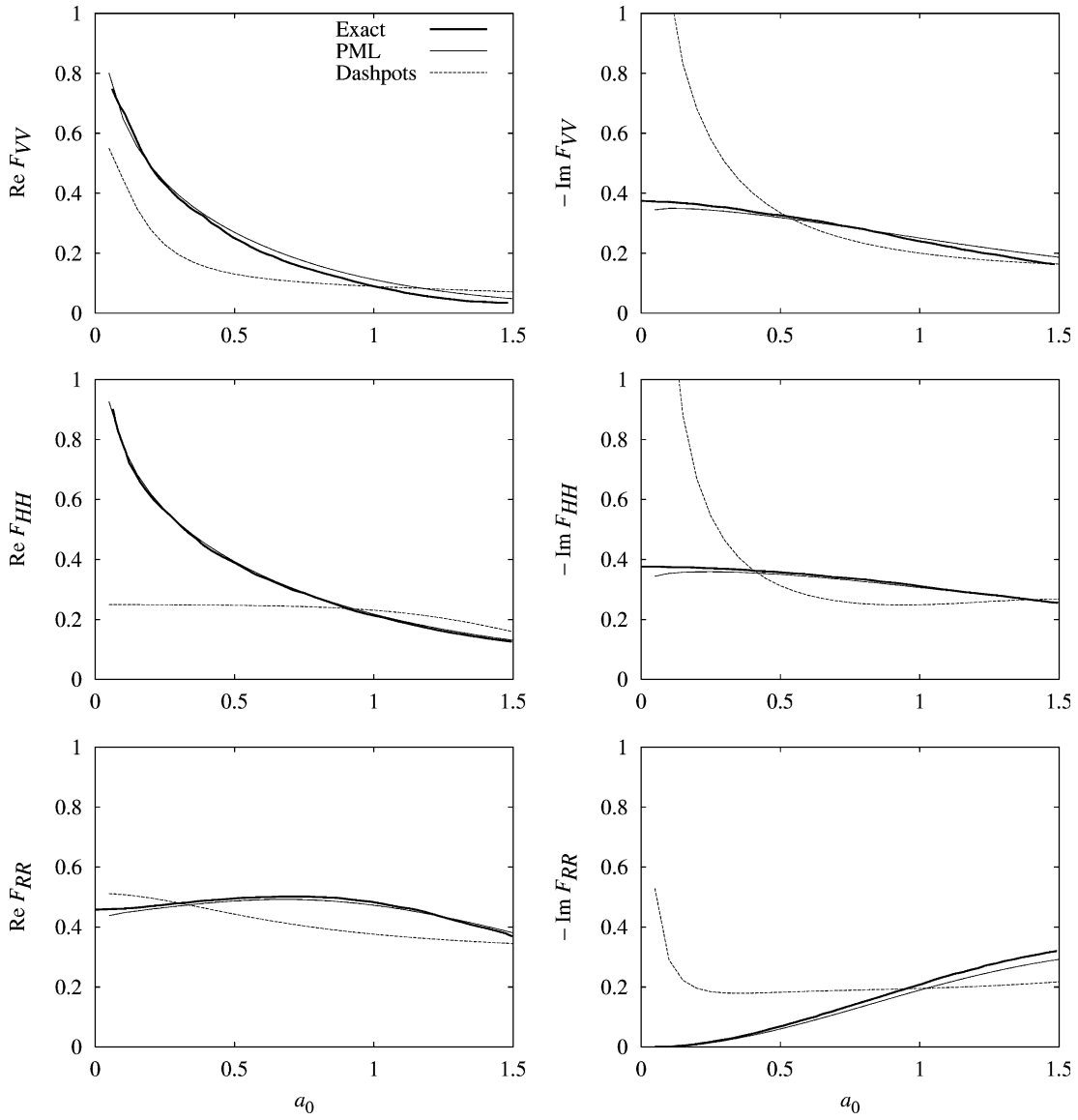

Fig. 15. Dynamic flexibility coefficients of rigid strip on elastic half-plane computed using a PML model as well as a viscous dashpot boundary model; $L = 3b/2$, $h = b/2$, $L_P = b$, $f_1(x_1) = 10\langle x_1 - h\rangle/L_P$, $f_2(x_2) = 10\langle |x_2| - L\rangle/L_P$; $\langle x\rangle := (x + |x|)/2$; $\mu = 1$, $v = 0.25$.

results from the PML model are highly accurate, even though the domain is too small for the dashpot model to produce accurate results for this viscoelastic medium.

Fig. 17(a) shows a cross-section of the rigid strip supported by a viscoelastic layer on a half-plane, and Fig. 17(b) shows a corresponding PML model where λ_i are of the form in Eq. (69) with linear attenuation functions in the PMLs. The PMLs employed for the layer and the half-plane have different moduli, corresponding to the moduli for the elastic media. For comparison, a viscous dashpot model is also employed, where the entire bounded domain is taken to be viscoelastic, and consistent dashpots replace the fixed outer boundary. Fig. 18 compares results from the PML model and from the dashpot model against semi-ana-

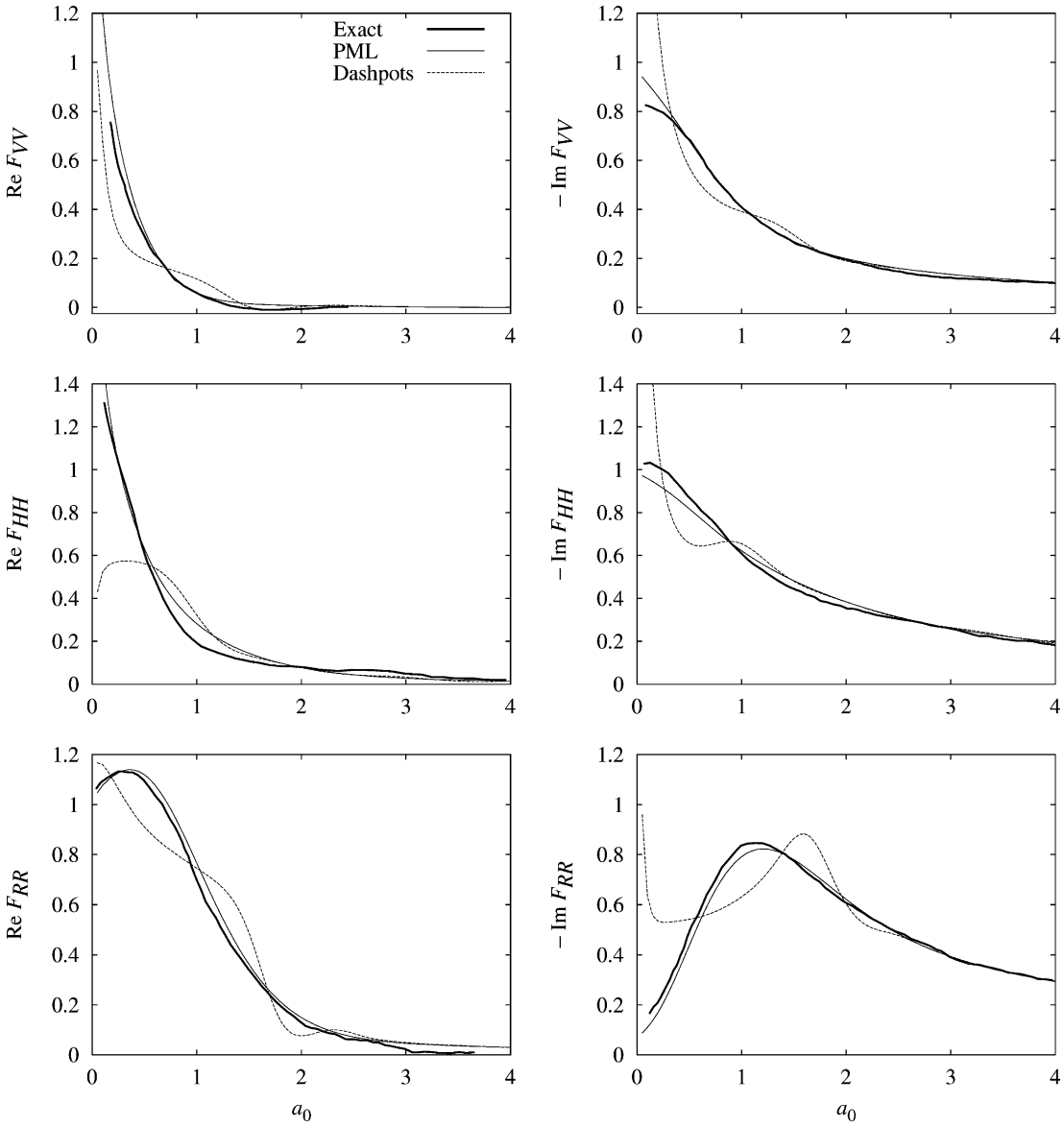

Fig. 16. Dynamic flexibility coefficients of rigid strip on viscoelastic half-plane computed using a PML model as well as a viscous dashpot boundary model; $L = 3b/2$, $h = b/2$, $L_P = b$, $f_1(x_1) = 10\langle x_1 - h\rangle/L_P$, $f_2(x_2) = 10\langle|x_2| - L\rangle/L_P$; $E = 1$, $v = 0.33$, $\zeta = 0.05$, $a_0 = \omega b/\sqrt{E/\rho}$.

lytical results [47,48]. The results from the PML model are reasonably accurate, even though the computational domain is small and the cost is comparable to that of the dashpot model. The smallness of the domain is evident in the inaccuracy of results from the dashpot model, especially for vertical and for horizontal motion.

Fig. 19(a) shows a cross-section of the rigid strip supported by a viscoelastic layer on a rigid base, and Fig. 19(b) shows a corresponding PML model where λ_i are of the form in Eq. (69) with $f_1(x_1) = 0$ and $f_2(x_2)$ linear in the PML. Fig. 20 presents results from the PML model and from a comparable viscous dashpot

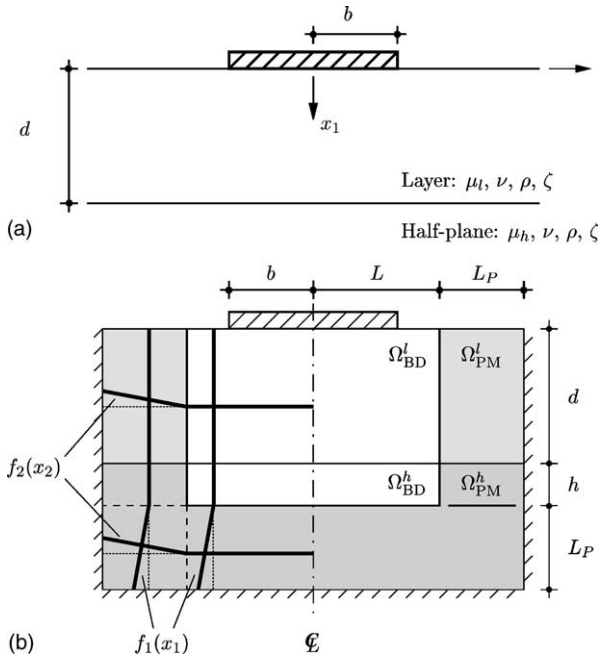

Fig. 17. (a) Cross-section of the rigid strip of half-width b on a homogeneous isotropic viscoelastic layer on half-plane; (b) a PML model.

model against semi-analytical results [47,48]. The PML model produces reasonably accurate results at a cost comparable to that of the dashpot model. The boundedness of the domain in the horizontal direction is made prominent by the gross inaccuracy of results for F_{HH} as computed from the dashpot model. Notably, accurate PML results are obtained for this waveguide system with significant evanescent modes. Thus, the stretching function of Eq. (69) is adequate for these evanescent modes, but with $f_i(L_P) = 20$, rather than the value of 10 used for other examples in this paper; a value of $f_i(L_P) = 10$ for this problem produces results that are slightly less accurate.

5. Conclusions

The concept of a PML has been developed in the context of time-harmonic elastodynamics by utilising insights obtained in the context of electromagnetics. The concept has been developed through the presentation of perfectly matched media for three different systems: (1) a rod on elastic foundation, (2) a continuum undergoing anti-plane motion, and (3) a continuum undergoing plane-strain or three-dimensional motion.

The PML concept is summarised as follows. A perfectly matched medium (PMM) is defined as one governed by a modification of the equations for the elastic medium, with the modification motivated by a continuous, complex-valued, uncoupled coordinate stretching. Solutions admitted by the PMM are of the form of those admitted by the elastic medium, but with the stretched coordinates replacing the real coordinates. PMMs exhibit the perfect matching property: if the stretching functions of two adjacent PMMs match at their interface, then the interface is invisible to all wave-type solutions in the PMMs and no reflected wave is generated when a wave travels from one PMM to the other. This property holds irrespective of the direction of propagation of the wave or its frequency. Furthermore, if choices of the

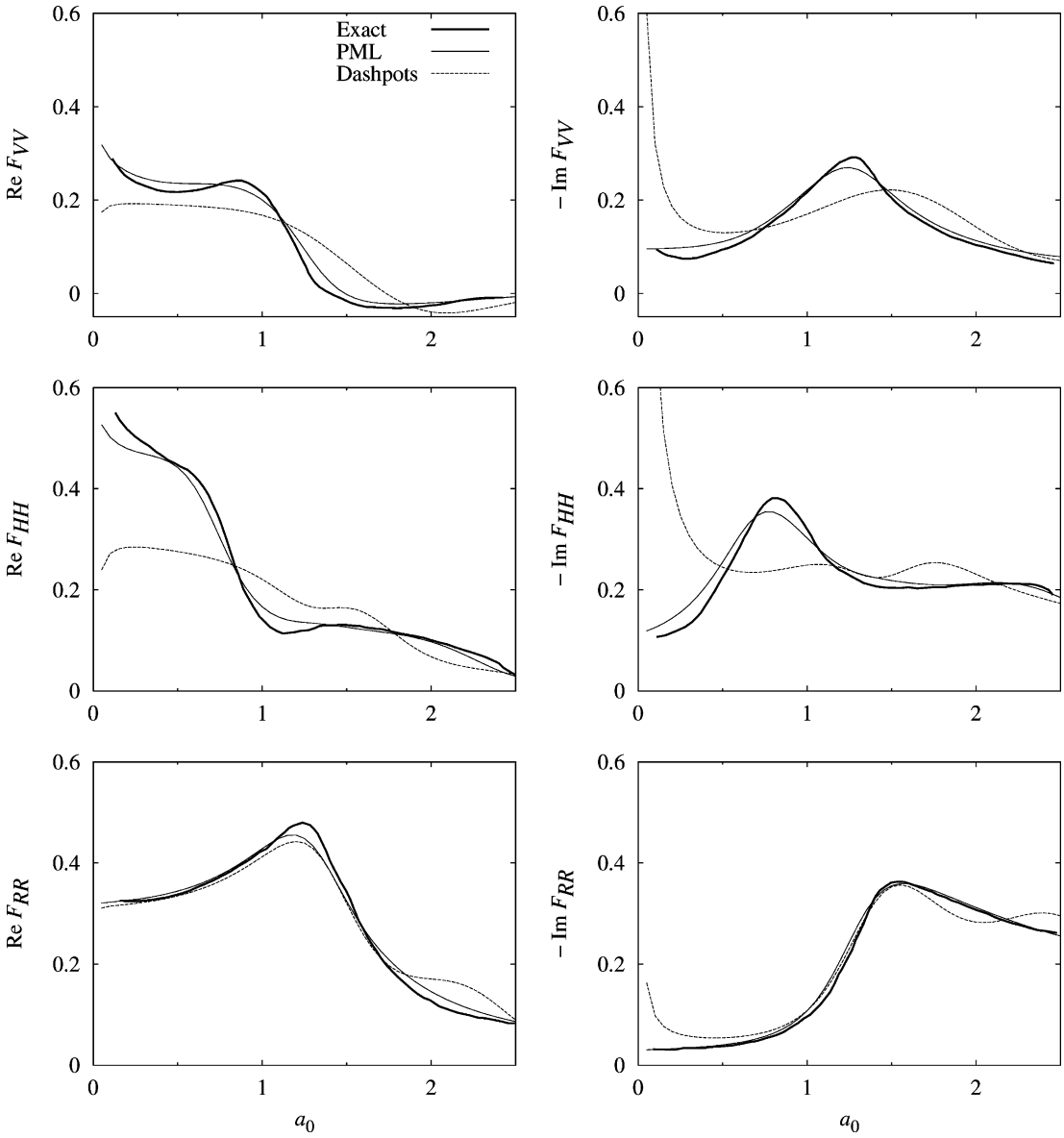

Fig. 18. Dynamic flexibility coefficients of rigid strip on viscoelastic layer on half-plane computed using a PML model as well as a viscous dashpot boundary model; $L = 3b/2$, $L_P = b$, $h = b/2$, $f_1(x_1) = 10\langle x_1 - (d+h)\rangle/L_P$, $f_2(x_2) = 10\langle |x_2| - L\rangle/L_P$; $d = 2b$, $\mu_h = 4\mu_l$, $\mu_l = 1$, $v = 0.4$, $\zeta = 0.05$, $a_0 = \omega b/\sqrt{\mu_l/\rho}$.

stretching functions are appropriate, the solutions in the PMM take the form of the corresponding elastic-medium solution, but with an imposed spatial attenuation. Realistic choices of the stretching function can impose attenuation on both propagating and evanescent waves. Notably, the imposed attenuation is directly spatial: it is not imposed through a temporal attenuation, or damping. The perfect matching and the attenuative properties of the PMM is employed to build an absorbing layer—the PML—around a bounded domain such that the layer absorbs and attenuates outward-propagating waves of all non-tangential angles-of-incidence and of all non-zero frequencies. Termination of the layer by a fixed boundary causes reflection

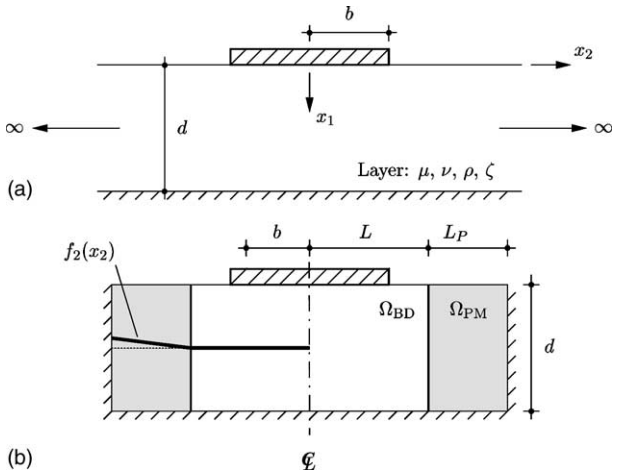

Fig. 19. (a) Cross-section of the rigid strip of half-width b on a homogeneous isotropic viscoelastic layer on rigid base; (b) a PML model.

of the waves back towards the bounded domain, with the amplitude of reflected waves controllable—independently of the size of the bounded domain—by the choice of the PML parameters: (a) the depth of the layer and (b) the attenuation profile in it. Thus, wave propagation in an unbounded domain can be modelled through a bounded domain that is restricted to the region of interest in the analysis, and a suitably-defined PML surrounding it.

The one-dimensional problem of the semi-infinite rod on elastic foundation has been used to analytically study a bounded-domain-PML model. The stretching function is expressed in terms of an attenuation function, which controls the reflection due to the finite depth of the PML. The reflection coefficient is related to the dynamic stiffness of the rod, and it is shown that the dynamic stiffness of the PML model approaches that of the unbounded-domain system as the reflection coefficient approaches zero. It is argued analytically that the attenuation function should be chosen to increase linearly from zero at the bounded-domain-PML interface to a maximum value at the end of the layer, and that this maximum value, as well as the depth of the layer, should be used to control the accuracy of results; this conclusion is validated through analytical results. It is expected that a rudimentary trial-and-error procedure should be sufficient to establish an adequate maximum value of the attenuation function. Also proposed is a realistic choice of the stretching function that does not employ prior knowledge of the frequency equation of the system, but is adequate for both evanescent and propagating waves; this adequacy is confirmed through analytical and numerical results.

It has been shown that the one-dimensional and the anti-plane PMM, although formulated through coordinate-stretching, can be also be interpreted as anisotropic, inhomogeneous viscoelastic media, echoing similar interpretations of electromagnetics PMLs [35,40]. These equivalent interpretations have then been used to obtain symmetric FE implementations of these PMMs, with the implementation of the anti-plane PMM matching those presented in earlier works [25,41]. The PMM for plane-strain or three-dimensional motion is not amenable to a similar equivalent interpretation; however, a novel displacement-based, symmetric FE implementation of this PMM is still obtained, by expressing the PMM equations in a tensorial form. The FE matrices obtained are symmetric, but intrinsically complex-valued and frequency-dependent. Thus the system matrices for the entire bounded domain are complex, symmetric and banded, the PML contributions to which have to be computed anew for each frequency.

These FE implementations have been applied to the following canonical problems: (1) the one-dimensional semi-infinite rod on elastic foundation, (2) the anti-plane motion of a semi-infinite layer on rigid base, and (3) the classical plane-strain soil–structure interaction problems of a rigid strip-footing on a

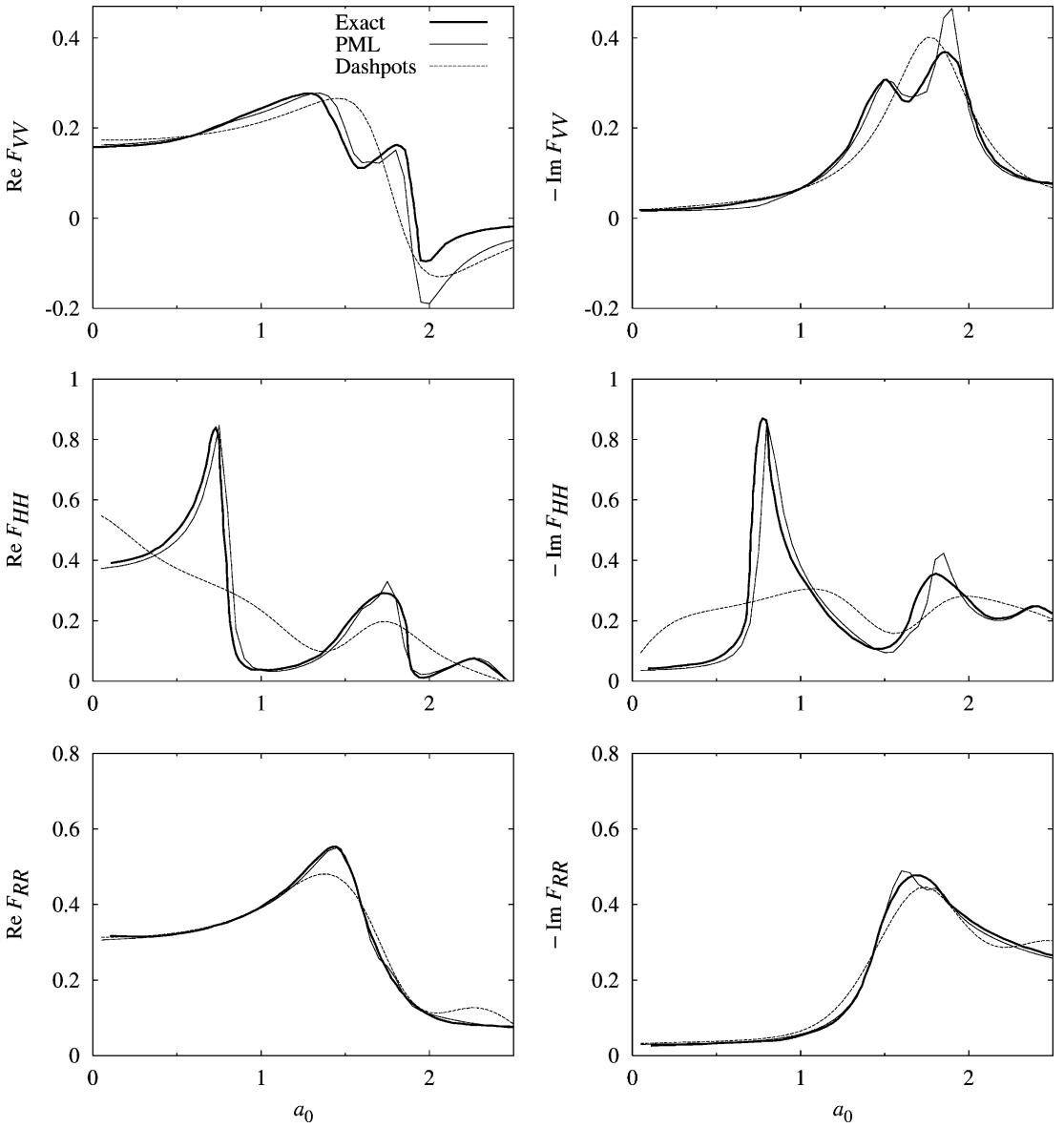

Fig. 20. Dynamic flexibility coefficients of rigid strip on viscoelastic layer on rigid base computed using a PML model as well as a viscous dashpot boundary model; $L = 3b/2$, $L_P = b$, $f_1(x_1) = 0$, $f_2(x_2) = 20\langle|x_2| - L\rangle/L_P$; $d = 2b$, $\mu = 1$, $v = 0.4$, $\zeta = 0.05$.

(i) half-plane, (ii) layer on a half-plane, and (iii) layer on a rigid base. Highly accurate results have been obtained from PML models using small bounded domains at low computational costs; the computational cost of the PML models was seen to be similar to that of comparable viscous dashpot models, and the inaccuracy of results from these dashpot models emphasized the small size of these bounded domains. Notably, accurate PML results have been obtained even for the waveguide system of a layer on a rigid base, undergoing either anti-plane or plane-strain motion, where evanescent modes are significant. This is achieved through the realistic choice of the stretching function proposed in the one-dimensional analysis;

such a stretching function is thus seen to be adequate even for systems with many evanescent modes. Preliminary numerical investigations of the effect of mesh density on the accuracy of results suggest that the mesh density in the PML should be chosen to be similar to that in the bounded domain, echoing conclusions reached by an earlier dispersion analysis [25].

This paper presents PMLs for homogeneous, isotropic media only. However, the same motivation of complex-valued coordinate stretching is utilised for all three systems to define the PMM corresponding to the elastic medium. Consequently (1) all three PMMs exhibit the perfect matching property, (2) propagating harmonic waveforms in the elastic medium are transformed to attenuated waveforms in the PMM, and (3) the constitutive relation is not affected by the coordinate-stretching, i.e., the constitutive relation in the PMM is the same as that in the elastic medium. These observations—especially the third—mirror similar ones made in the context of electromagnetic waves [34,36,49], where PMLs have been formulated for anisotropic, inhomogeneous media [36], underscoring the possibility of extending these elastodynamic PML formulations to anisotropic, continuously-inhomogeneous elastic media with at most minimal modifications. In fact, the PMMs presented in this paper, as well as any such extensions, could be seen as verifications of an assertion by Teixeira and Chew [35]. They provide a geometric interpretation of the PML concept, as a change in the metric of the coordinate space, and state: "...the PML concept does not depend on the particular form of field equations and is applicable to any linear wave phenomena."

Acknowledgements

This research investigation is funded by the Waterways Experiment Station, US Army Corps of Engineers, under Contract DACW39-98-K-0038; this financial support is gratefully acknowledged. The authors are also grateful to Prof. Robert L. Taylor, Prof. Sanjay Govindjee, Prashanth K. Vijalapura, Antar Bandyopadhyay and Prof. Fernando L. Teixeira for their helpful advice and comments, and to Claire Johnson for editing the manuscript. The authors are grateful to an anonymous reviewer whose comments led to improvements in the manuscript.

References

[1] D. Givoli, Numerical Methods for Problems in Infinite Domains, Elsevier, Amsterdam, 1992.
[2] S.V. Tsynkov, Numerical solution of problems on unbounded domains: A review, Appl. Numer. Math. 27 (4) (1998) 465–532.
[3] J.P. Wolf, Dynamic Soil–Structure Interaction, Prentice-Hall, Englewood Cliffs, NJ, 1985.
[4] H. Bao, J. Bielak, O. Ghattas, L.F. Kallivokas, D.R. O'Hallaron, J.R. Shewchuck, J. Xu, Large-scale simulation of elastic wave propagation in heterogeneous media on parallel computers, Comput. Methods Appl. Mech. Engrg. 152 (1–2) (1998) 85–102.
[5] G.D. Manolis, D.E. Beskos, Boundary Element Methods in Elastodynamics, Unwin Hyman, London, 1988.
[6] D. Givoli, J.B. Keller, Non-reflecting boundary conditions for elastic waves, Wave Motion 12 (3) (1990) 261–279.
[7] D. Givoli, S. Vigdergauz, Artificial boundary conditions for 2D problems in geophysics, Comput. Methods Appl. Mech. Engrg. 110 (1–2) (1993) 87–101.
[8] C. Song, J.P. Wolf, The scaled boundary finite-element method—alias consistent infinitesimal finite-element cell method—for elastodynamics, Comput. Methods Appl. Mech. Engrg. 147 (3–4) (1997) 329–355.
[9] J. Lysmer, R.L. Kuhlemeyer, Finite dynamic model for infinite media, J. Engrg. Mech. Div., ASCE 95 (EM4) (1969) 859–877.
[10] R. Clayton, B. Engquist, Absorbing boundary conditions for acoustic and elastic wave equations, Bull. Seismol. Soc. Am. 67 (6) (1977) 1529–1540.
[11] R.L. Higdon, Absorbing boundary conditions for elastic waves, Geophysics 56 (2) (1991) 231–241.
[12] D. Givoli, J.B. Keller, Special finite elements for use with high-order boundary conditions, Comput. Methods Appl. Mech. Engrg. 119 (3–4) (1994) 199–213.
[13] D. Givoli, High-order nonreflecting boundary conditions without high-order derivatives, J. Computat. Phys. 170 (2) (2001) 849–870.
[14] M. Israeli, S.A. Orszag, Approximation of radiation boundary conditions, J. Computat. Phys. 41 (1) (1981) 115–135.
[15] C. Cerjan, D. Kosloff, R. Kosloff, M. Reshef, A nonreflecting boundary-condition for discrete acoustic and elastic wave-equations, Geophysics 50 (4) (1985) 705–708.

[16] J. Sochaki, R. Kubichek, J. George, W.R. Fletcher, S. Smithson, Absorbing boundary conditions and surface waves, Geophysics 52 (1) (1987) 60–71.
[17] T. Furumura, H. Takenaka, A wraparound elimination technique for the pseudospectral wave synthesis using an antiperiodic extension of the wavefield, Geophysics 60 (1) (1995) 302–307.
[18] W.D. Smith, A nonreflecting plane boundary for wave propagation problems, J. Computat. Phys. 15 (4) (1974) 492–503.
[19] F. Medina, J. Penzien, Infinite elements for elastodynamics, Earthquake Engrg. Struct. Dyn. 10 (5) (1982) 699–709.
[20] C.-B. Yun, D.-K. Kim, J.-M. Kim, Analytical frequency-dependent infinite elements for soil–structure interaction analysis in two-dimensional medium, Engrg. Struct. 22 (3) (2000) 258–271.
[21] J.-P. Bérenger, A perfectly matched layer for the absorption of electromagnetic waves, J. Computat. Phys. 114 (2) (1994) 185–200.
[22] W.C. Chew, W.H. Weedon, A 3D perfectly matched medium from modified Maxwell's equations with stretched coordinates, Microw. Opt. Technol. Lett. 7 (13) (1994) 599–604.
[23] Q. Qi, T.L. Geers, Evaluation of the perfectly matched layer for computational acoustics, J. Computat. Phys. 139 (1) (1998) 166–183.
[24] E. Turkel, A. Yefet, Absorbing PML boundary layers for wave-like equations, Appl. Numer. Math. 27 (4) (1998) 533–557.
[25] I. Harari, M. Slavutin, E. Turkel, Analytical and numerical studies of a finite element PML for the Helmholtz equation, J. Computat. Acoust. 8 (1) (2000) 121–137.
[26] F.Q. Hu, On absorbing boundary conditions for linearized Euler equations by a perfectly matched layer, J. Computat. Phys. 129 (1) (1996) 201–219.
[27] Y.Q. Zeng, J.Q. He, Q.H. Liu, The application of the perfectly matched layer in numerical modeling of wave propagation in poroelastic media, Geophysics 66 (4) (2001) 1258–1266.
[28] W.C. Chew, Q.H. Liu, Perfectly matched layers for elastodynamics: A new absorbing boundary condition, J. Computat. Acoust. 4 (4) (1996) 341–359.
[29] F.D. Hastings, J.B. Schneider, S.L. Broschat, Application of the perfectly matched layer (PML) absorbing boundary condition to elastic wave propagation, J. Acoust. Soc. Am. 100 (5) (1996) 3061–3069.
[30] Q.H. Liu, Perfectly matched layers for elastic waves in cylindrical coordinates, J. Acoust. Soc. Am. 105 (4) (1999) 2075–2084.
[31] Y.-G. Zhang, J. Ballmann, Two techniques for the absorption of elastic waves using an artificial transition layer, Wave Motion 25 (1) (1997) 15–33.
[32] F. Collino, C. Tsogka, Application of the perfectly matched absorbing layer model to the linear elastodynamic problem in anisotropic heterogeneous media, Geophysics 66 (1) (2001) 294–307.
[33] E. Bécache, P. Joly, C. Tsogka, Fictitious domains, mixed finite elements and perfectly matched layers for 2-D elastic wave propagation, J. Computat. Acoust. 9 (3) (2001) 1175–1201.
[34] W.C. Chew, J.M. Jin, E. Michielssen, Complex coordinate stretching as a generalized absorbing boundary condition, Microw. Opt. Technol. Lett. 15 (6) (1997) 363–369.
[35] F.L. Teixeira, W.C. Chew, Unified analysis of perfectly matched layers using differential forms, Microw. Opt. Technol. Lett. 20 (2) (1999) 124–126.
[36] F.L. Teixeira, W.C. Chew, A general approach to extend Berenger's absorbing boundary condition to anisotropic and dispersive media, IEEE Trans. Antenn. Propag. 46 (9) (1998) 1386–1387.
[37] D.R. Bland, The Theory of Linear Viscoelasticity, Pergamon Press, New York, 1960.
[38] T.J.R. Hughes, The Finite Element Method: Linear Static and Dynamic Finite Element Analysis, Dover, NY, 2000.
[39] K.F. Graff, Wave Motion in Elastic Solids, Dover, NY, 1975.
[40] Z.S. Sacks, D.M. Kingsland, R. Lee, J.-F. Lee, A perfectly matched anisotropic absorber for use as an absorbing boundary condition, IEEE Trans. Antenn. Propag. 43 (12) (1995) 1460–1463.
[41] F. Collino, P. Monk, The perfectly matched layer in curvilinear coordinates, SIAM J. Sci. Comput. 19 (6) (1998) 2061–2090.
[42] J.P. Wolf, C. Song, Finite-Element Modelling of Unbounded Media, Wiley, Chichester, England, 1996.
[43] J. De Moerloose, M.A. Stuchly, Behaviour of Bérenger's ABC for evanescent waves, IEEE Microw. Guided Wave Lett. 5 (10) (1995) 344–346.
[44] J.-P. Bérenger, Application of the CFS PML to the absorption of evanescent waves in waveguides, IEEE Microw. Wireless Compon. Lett. 12 (6) (2002) 218–220.
[45] J.E. Luco, R.A. Westmann, Dynamic response of a rigid footing bonded to an elastic half space, J. Appl. Mech., ASME 39 (2) (1972) 527–534.
[46] G. Gazetas, Importance of soil anisotropy on foundation displacement functions, in: Advances in Geotechnical Earthquake Engineering, vol. 3, University of Missouri, Rolla, 1981, pp. 1039–1046.
[47] G. Gazetas, J.M. Roesset, Vertical vibration of machine foundations, J. Geotech. Engrg. Div., ASCE 105 (12) (1979) 1435–1454.
[48] G. Gazetas, J.M. Roesset, Forced vibrations of strip footings on layered soils, in: Methods of Structural Analysis, vol. 1, ASCE, 1976, pp. 115–131.
[49] F.L. Teixeira, W.C. Chew, Complex space approach to perfectly matched layers: A review and some new developments, Int. J. Numer. Modell.: Electron. Networks, Dev. Fields 13 (5) (2000) 441–455.